Chemotaxis and autoinducer-2 signalling mediate colonization and contribute to co-existence of Escherichia coli strains in the murine gut

Journal Article

Author(s):
Laganenka, Leanid; Lee, Jae-Woo; Malfertheiner, Lukas; Dieterich, Cora Lisbeth; Fuchs, Lea; Piel, Jörn; von Mering, Christian; Sourjik, Victor; Hardt, Wolf-Dietrich

Publication date:
2023-02

Permanent link:
https://doi.org/10.3929/ethz-b-000596863

Originally published in:
Nature Microbiology 8(2), https://doi.org/10.1038/s41564-022-01286-7

Funding acknowledgement:
173338 - Deciphering the initial steps that lead to Salmonella Typhimurium diarrhea (SNF)
192567 - Mechanisms controlling the Salmonella Typhimurium gut infection (SNF)

Chemotaxis and autoinducer-2 signalling enhance gut colonization and contribute to niche segregation of *Escherichia coli* strains in the mammalian gut

Leanid Laganenka[1], Jae-Woo Lee[2], Lukas Malfertheiner[3], Cora Lisbeth Dieterich[1], Lea Fuchs[1], Jörn Piel[1], Christian von Mering[3], Victor Sourjik[2], Wolf-Dietrich Hardt[1]

[1]*Institute of Microbiology, D-BIOL, ETH Zurich, Zurich, Switzerland*

[2]*Max Planck Institute for Terrestrial Microbiology and Center for Synthetic Microbiology (SYNMIKRO), Marburg, Germany*

[3]*Department of Molecular Life Sciences and SIB Swiss Institute of Bioinformatics, University of Zurich, Zurich, Switzerland*

Corresponding author: Wolf-Dietrich Hardt, hardt@micro.biol.ethz.ch

Abstract

Bacteria communicate and coordinate their behavior by producing and sensing extracellular small molecules called autoinducers. The astounding structural diversity of these molecules allows bacteria to synchronize their behavior on both intra- and interspecies levels. Autoinducer 2 (AI-2) is produced and detected by a variety of bacteria, thus principally allowing interspecies communication. Although AI-2 is a major autoinducer molecule present in the mammalian gut, its role in bacteria-bacteria and bacteria-host interactions during gut colonization remains elusive. Here, we show that chemotaxis and AI-2 signalling promote gut colonization by *Escherichia coli*, which is in turn connected to the ability of the bacteria to utilize fructoselysine. We further show that the genomic diversity of *E. coli* strains with respect to AI-2 signaling allows ecological niche segregation and stable co-existence of different *E. coli* strains in the mammalian gut.

Introduction

Chemotaxis allows motile bacteria to navigate in chemical gradients. Although being a costly cellular behaviour, chemotaxis provides bacteria with physiological advantage by enhancing access to nutrient and energy sources[1–3]. Furthermore, it facilitates detection and colonization of beneficial niches by free-living and host-associated bacteria, including plant and human pathogens[4]. In the latter case, some sensed compounds might serve as orientation cues within the host, even if they lack a direct metabolic value. These include hormones,

neurotransmitters, acids, and other compounds[4–7]. However, despite the ever-growing mechanistic understanding of chemotaxis systems and the range of molecules sensed by them in diverse bacteria, the ecological role of chemotaxis has received much less attention[8–10]. The physiological importance of chemotaxis has remained incompletely understood even for well-established model organisms such as *E. coli*. To our knowledge, only one study addressed this question, finding that neither motility nor chemotaxis are required for gut colonization of *E. coli* F-18[11]. However, this strain was shown to lose motility during growth in the mouse large intestine, which was associated with mutations in the regulatory region of *flhDC* operon[12]. Besides leading to loss of flagella, these mutations further resulted in beneficial pleiotropic metabolic effects, making it impossible to draw any conclusions about the role of chemotaxis in motile *E. coli*.

Recent *ex vivo* studies have shown that collective behaviours of *E. coli* such as autoaggregation and biofilm formation are dependent on chemotaxis towards the interspecies quorum sensing signal autoinducer-2 (AI-2)[13–15]. Self-produced AI-2 attracts bacteria towards the growing aggregates, and it further enhances mature biofilm formation in a chemotaxis-dependent manner. AI-2 is produced and sensed by a vast number of bacterial species, and AI-2 mimics were reported to be synthesized by eukaryotic cells[16–18]. The chemotactic response to AI-2 has been clearly shown for several bacterial species, and it is apparently not restricted to AI-2-producing bacteria, suggesting its important role in establishing complex multispecies communities[19,20]. Indeed, AI-2 seems to affect bacterial community structure of the mammalian gut after antibiotic-induced dysbiosis and to promote colonization resistance to certain enteric pathogens[21,22]. However, there are still fundamental mechanistic gaps in our knowledge of how bacteria might benefit from AI-2 signalling under physiologically relevant conditions.

Here we studied the roles of chemotaxis and AI-2 signalling in *E. coli* gut colonization. We show that chemotaxis towards self-produced AI-2 provides *E. coli* with a fitness advantage during gut colonization, and that this hinges on fructoselysine metabolism. We further report the novel role of AI-2 chemotaxis in contributing to niche segregation and thus to co-existence of different *E. coli* strains in the gut based on their ability to perform AI-2 chemotaxis. These findings might be relevant for other AI-2 chemotactic bacteria in their natural habitats.

Results

Chemotaxis provides *E. coli* with a fitness advantage during gut colonization. To assess the role of chemotaxis in gut colonization by *E. coli*, we infected ampicillin-pretreated specific pathogen-free (SPF) mice with a 1:1 mixture of *E. coli* Z1331 wild-type strain, a motile stool isolate from a healthy human volunteer[23], and its non-chemotactic Δ*cheY* derivative (Fig.

1a). A wild-type *E. coli* isolate was chosen over the classical K-12 laboratory strain since the accumulation of lab cultivation-derived mutations might result in overall loss of fitness during the gut colonization and thus compromise the physiological relevance of the study[24–27]. Since SPF mice are normally resistant to *E. coli* colonization, antibiotic pretreatment is required to transiently suppress resident gut microbiota, thus allowing for gut luminal *E. coli* colonization[28]. Levels of *E. coli* colonization and relative fitness of the WT and Δ*cheY* strains were determined by differential plating of faeces collected at several time points within 72 h.p.i.. *E. coli* Z1331 colonized the gut of the mice within 8 h.p.i. at densities of ≈10^9 c.f.u./g stool and remained at carrying capacity throughout the course of the experiment (Extended Data Fig. 1a). In competitive infections with a 1:1 inoculum, Δ*cheY* knockout cells were consistently outcompeted by up to 50-fold by the wild-type strain, indicating that chemotaxis is required for successful gut colonization by *E. coli* Z1331 (Fig. 1b, see Materials and Methods for the rationale for using competitive infections). This phenotype was observed along the whole length of the small and the large intestine at 72 h.p.i. (Fig. 1c), indicating that the competitive fitness advantage provided by chemotaxis is not limited to a particular region of the mouse gut. Interestingly, although in *Salmonella enterica* serovar Typhimurium, a close relative of *E. coli*, the beneficial role of chemotaxis only becomes apparent at high levels of gut inflammation[29,30], this was not the case for *E. coli* Z1331 in our experiments. The Lipocalin-2 level, a marker of gut inflammation, remained within the range of concentrations characteristic for unperturbed mice during the entire *E. coli* colonization experiment (Extended Data Fig. 1b). Notably, a similar loss of fitness was observed for a Δ*cheY* knockout mutant of *E. coli* K-12 W3110 as well as for several other *E. coli* isolates from different phylogroups (Extended Data Fig. 1c). These results suggest that the competitive colonization benefit provided by chemotaxis might be not strictly strain-specific, but rather of general importance for motile *E. coli* strains.

To visualize the spatial distribution of the WT and Δ*cheY* cells in the gut by confocal microscopy, we infected mice with the WT and Δ*cheY* cells that constitutively express mCherry and GFP, respectively. At 72 h.p.i., ileal, caecal and proximal colon tissues were excised and fixed in 4% paraformaldehyde. Subsequently, 10 µm tissue sections were additionally stained with DAPI and phalloidin to visualize the host tissue. As seen in Fig. 1d, WT cells appeared to form clusters reminiscent of the previously described aggregates[14], whereas much less aggregate formation was observed for Δ*cheY* cells (Fig. 1d, e; Extended Data Fig. 2). Less aggregation of Δ*cheY* knockout was also observed in single-strain infections, where no colonization defect of Δ*cheY* was detected (Extended Data Fig. 3). Our results suggest that chemotaxis contributes to gut colonization and spatial organization of *E. coli* cells in the gut.

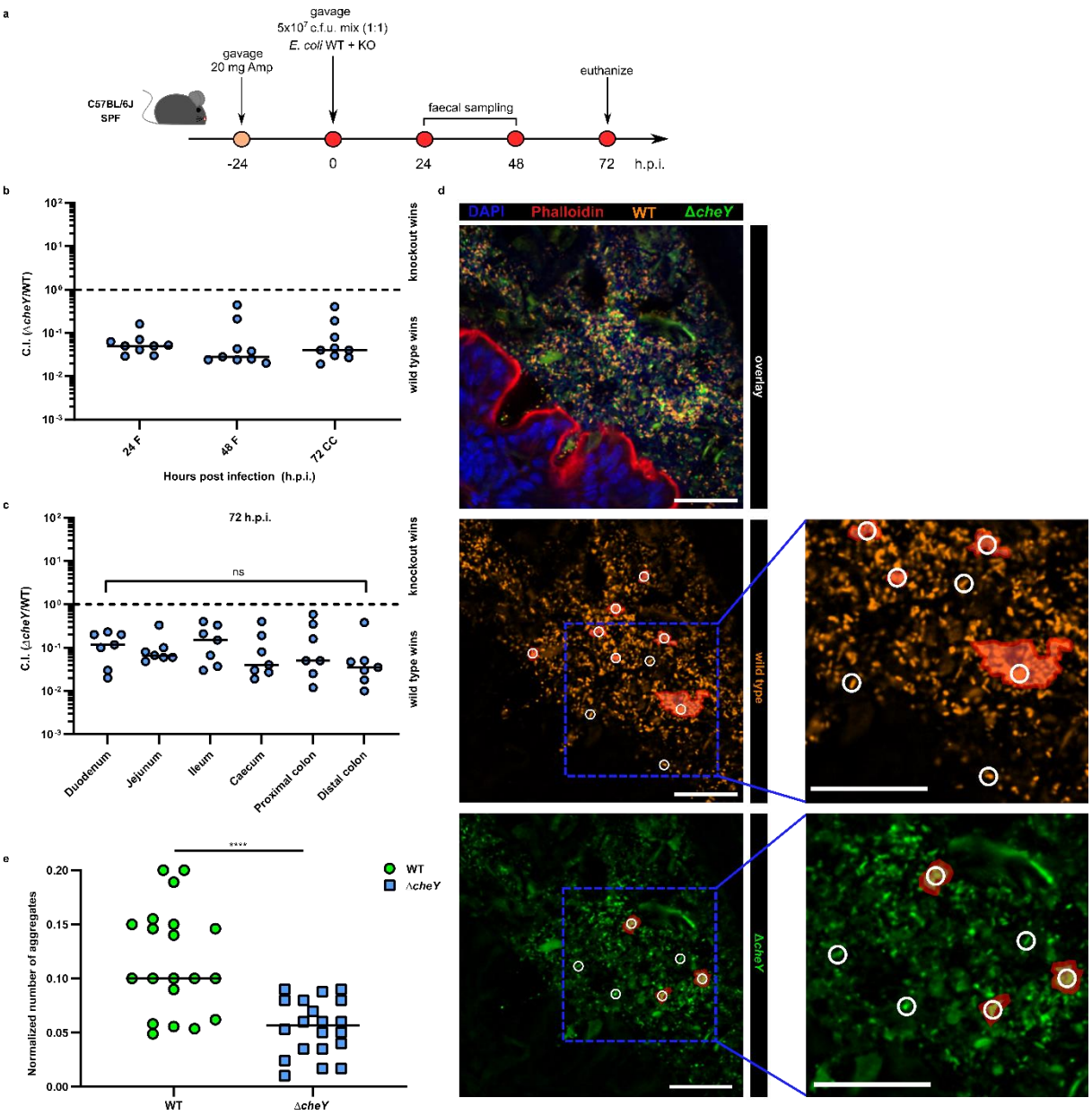

Figure 1. Chemotaxis provides *E. coli* with fitness advantage in competitive mouse infections. **a**, Experimental scheme of competitive infection. C57BL/6J specific pathogen-free (SPF) mice were pretreated with 20 mg ampicillin by oral gavage 24 h prior to infection with *E. coli* (1:1 mix WT and KO strain). Faeces were collected at 24, 48 h.p.i., unless stated otherwise, and mice were euthanized at 72 h.p.i. **b**, Competitive index (C.I.) of non-chemotactic Δ*cheY* (Z7741, unless stated otherwise) mutant in Δ*cheY*/WT competitive infection. F, faeces, CC, caecal content. Lines indicate median values (n=9, at least two independent replicates). **c**, C.I. values of Δ*cheY* in Δ*cheY*/WT competitive infection along the gut at 72 h.p.i. Lines indicate median values (n=7, at least two independent replicates). *P* values were analyzed using one-way ANOVA test (ns, not significant). **d**, Caecal tissue sections of mice infected with *E. coli* WT (mCherry-positive, shown in orange) and Δ*cheY* (Z7730, GFP-positive, shown in green) at 72 h.p.i (Δ*cheY*/WT C.I.=0.16). Actin filaments (red) and DNA (blue) were stained with phalloidin and DAPI, respectively. White circles indicate the threshold area (~50 px^2) for

adjacent cells (~10 px^2 in size) to be considered an aggregate. Examples of such aggregates are highlighted in red. Scale bars, 50 µm. **e**, Number of aggregates formed by WT and Δ*cheY* cells normalized to the number of detected cells in a tissue section (Mann-Whitney test, ****P<0.0001). Lines indicate median values (n=20, tissues sections from two independent experiments were analyzed).

Chemotaxis towards self-produced AI-2 enhances gut colonization by *E. coli*. As stated above, the clusters of *E. coli* cells observed in the gut tissue sections were similar to the aggregates formed by swimming *E. coli* cells in liquid medium. Since aggregation *ex vivo* was shown to be dependent on chemotaxis towards self-produced AI-2[14], we hypothesized that AI-2 chemotaxis might as well play a role during gut colonization. AI-2 is known to be produced and sensed by variety of both Gram-positive and Gram-negative bacteria[16], and a substantial number of gut-associated bacteria encode LuxS, the AI-2 synthase enzyme, potentially rendering AI-2 the most abundant interspecies quorum-sensing molecule in the gut[31]. *Ex vivo*, *E. coli*, chemotaxis towards AI-2 has been previously shown to control such group behaviours as autoaggregation and biofilm formation[14,15,32,33]. In contrast, its role *in vivo* remained unclear.

When extracellular AI-2 exceeds a certain threshold *ex vivo*, *E. coli* strains activate expression of the *lsr* operon, which contains genes required for AI-2 import (via an ABC transporter) and degradation. The LsrB protein binds AI-2 in the periplasm and directs its import via the LsrACD ABC transporter[34,35]. Additionally, AI-2-bound LsrB elicits a chemotactic response of *E. coli* cells to AI-2 by binding to the Tsr chemoreceptor[36]. As no chemotaxis-independent AI-2-related phenotypes have been observed in *E. coli*[13], deletion of the *lsrB* gene alone should be sufficient to abolish chemotaxis to AI-2 and AI-2-mediated phenotypes *in vitro*. Interestingly, ampicillin pretreatment of the SPF mice resulted in the transient increase of luminal AI-2 levels at 24 h post treatment, possibly due to the lysis of the resident microbial cells or shifts in the microbiota composition towards AI-2 producing bacteria (Extended Data Fig. 4a, b). As we could further detect *lsr* operon expression by *E. coli* Z1331 in the mouse gut lumen (Fig. 2a), we decided to explore the function of LsrB in gut colonization. Similar to the Δ*cheY* knockout, WT cells consistently outcompeted the isogenic Δ*lsrB* mutant in SPF mice already after 24 h.p.i. (Fig. 2b). In contrast, no fitness defect was observed for the Δ*lsrC* and Δ*lsrD* knockouts, indicating that the Δ*lsrB* phenotype is indeed attributable to the lack of chemotaxis towards AI-2, rather than impaired AI-2 import. Loss of chemotaxis towards AI-2 similarly affected the fitness of *E. coli* K-12 W3110 and 8850, other *lsr* operon-encoding isolates (Extended Data Fig. 5).

To further test our hypothesis, we took advantage of a well-established AI-2 overproducing *E. coli* strain (ARO071)[21]. Since AI-2 is sensed indirectly via an AI-2 binding protein LsrB, a narrow sensitivity range would be expected due to saturation of the receptors

at high background stimulation[37]. Increasing luminal AI-2 concentrations by introducing *E. coli* ARO071 should thus saturate the chemotactic response and eliminate the advantage of the WT in a competitive infection. To test this, we again infected mice with a 1:1 mix of the WT *E. coli* Z1331and its isogenic Δ*lsrB* mutant. Although Δ*lsrB* was again stably outcompeted by the WT at 24 and 48 h.p.i. (C.I.≈10^{-1}), introducing the AI-2-overproducing strain at 48 h.p.i. abolished the competitive advantage of the WT strain within one day (C.I.≈1; Fig. 2c, d; Extended Data Fig. 4b, c). This was apparently related to a slight (though not significant) rise in the stool density of the Δ*lsrB* mutant that may go along with a very slight decrease in WT *E. coli* Z1331 densities (which is again not significant in our experiment). Regardless, we hypothesize that the observed shift in the C.I. values is attributable to the dynamic nature of the favourable niches in the gut. Any *E. coli*-occupied niche, in the mucus layer or in the gut lumen, is constantly washed out and renewed. Therefore, such niches must be constantly re-occupied by the respective strains. Abolishing AI-2 chemotaxis by saturating luminal AI-2 concentrations after two days of the competitive infection results in both wild-type and Δ*lsrB* strains having the same chance of establishing themselves in the newly opened niches by means of random motility. Furthermore, the dispersal of the wild-type *E. coli* from the existing niches (like the aggregates and biofilms of *E. coli* disperse upon addition of saturating AI-2 concentrations *in vitro*[14]) might also contribute to this process. Upon addition, *E. coli* ARO071 might also compete transiently with *E. coli* Z1331 WT for a niche that was previously accessible to this strain, and might thereby contribute to Δ*lsrB* reaching WT *E. coli* Z1331 densities.

Our further analysis showed that Δ*cheY* or Δ*cheY* Δ*lsrB* featured the same competitive defect against the wild-type strain, while Δ*lsrB* or Δ*cheY* were about as competitive as Δ*cheY* Δ*lsrB* (Extended Data Fig. 6). These results strongly suggest that chemotaxis towards AI-2 enhances gut colonization by *E. coli*. Interestingly, we noticed a minor fitness defect of Δ*cheY* in the Δ*lsrB* vs. Δ*cheY* Δ*lsrB* infection (Extended Data Fig. 6). Altogether, our observations suggest that AI-2 is the major chemoeffector, albeit not the only one, contributing to chemotaxis-driven gut colonization of ampicillin-pretreated SPF mice by *E. coli*.

It has been recently shown that AI-2 mimics can be produced by eukaryotic cells: by *Saccharomyces cerevisiae* and, more intriguingly, by intestinal epithelial cells[17,18]. This suggests that there are three potential sources of AI-2-type molecules in the gut which might affect *E. coli* colonization in our experiments: epithelium-, microbiota-, or self-produced signals. We therefore aimed at pinpointing the major source of AI-2 or AI-2 mimics sensed by the *E. coli* Z1331 cells. To distinguish between host- and self-produced molecules, we investigated the role of LsrB during gut colonization of germ-free (GF) mice in WT *E. coli* Z1331 and an isogenic strain incapable of AI-2 production (*E. coli* Z1331 Δ*luxS*). As in the case of ampicillin-pretreated SPF mice, Δ*lsrB* was outcompeted by the WT strain in GF mice (without antibiotic pretreatment; Extended Data Fig. 7a, b). However, no advantage of LsrB was observed when

both strains were lacking *luxS.* Thus, it is not epithelium-derived, but self-produced AI-2 that is involved in colonization. In agreement with this explanation, no accumulation of the WT cells was observed close the epithelial tissue (Fig. 1d, e).

Although antibiotic treatment leads to suppression of resident microbiota and stochastic loss of bacterial phyla in SPF mice, the microbiota is never completely cleared by the antibiotic and regrows within several days after the treatment[38]. It was thus interesting to see whether AI-2 produced by residual microbiota may contribute to the LsrB-mediated phenotype in *E. coli* Z1331. To answer this question, we repeated the experiment described above in ampicillin-pretreated SPF mice. Again, no fitness loss was observed for Δ*lsrB* Δ*luxS* vs Δ*luxS*, suggesting that self-produced AI-2 that is sensed by *E. coli* during gut colonization confers the competitive advantage in all our initial experiments (Extended Data Fig. 7c, d).

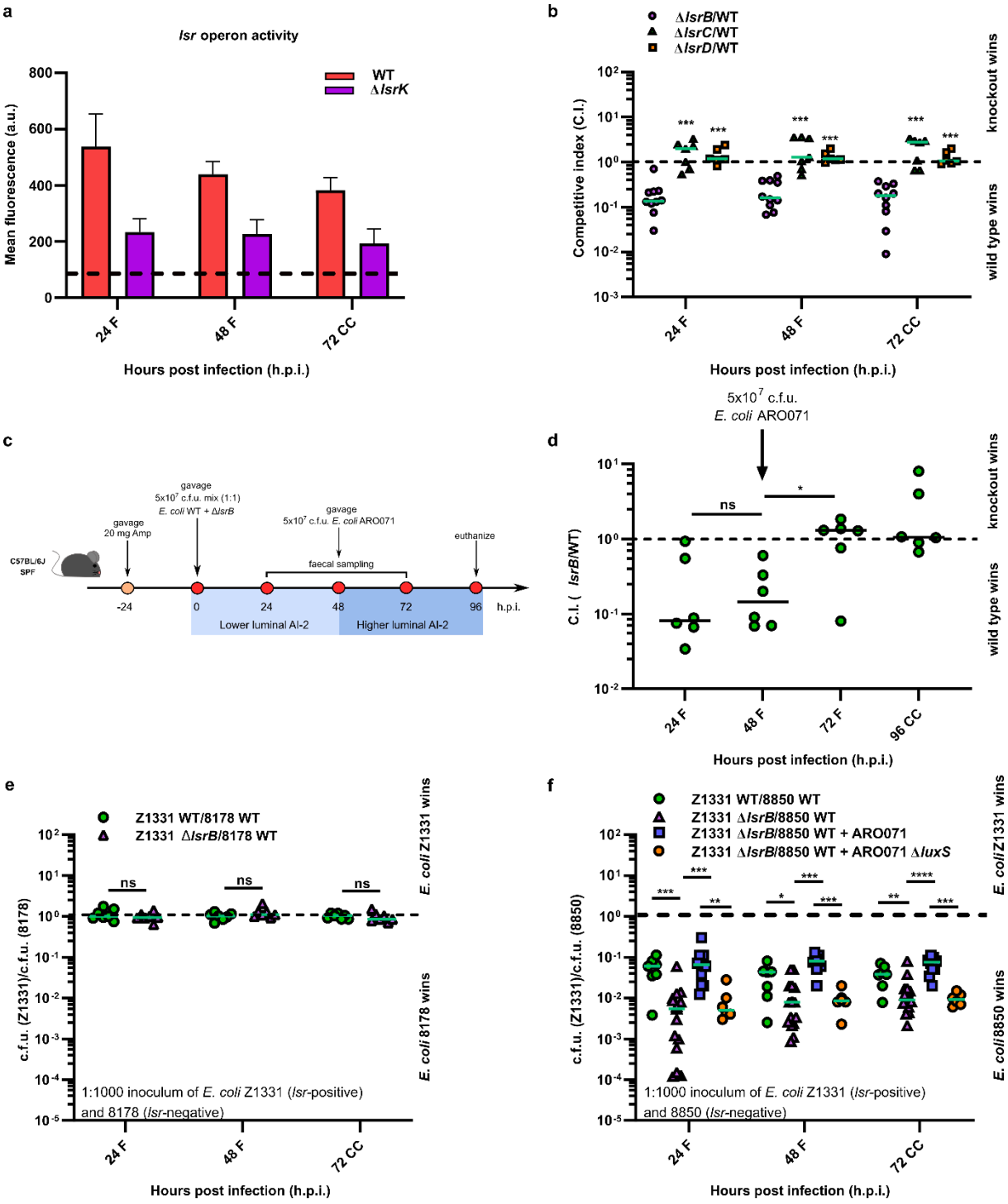

Figure 2. Chemotaxis towards AI-2 promotes colonization and drives ecological niche segregation of *E. coli* strains in the gut. a, *In vivo lsr* promoter activity in wild-type *E. coli* cells transformed with pUA66::P*lsr*-gfp, as measured by flow cytometry and expressed in arbitrary units (a.u.). Δ*lsrK* strain (no activation of *lsr* operon) was used as a negative control. Error bars indicate s.d. (n=5, at least two independent replicates). Dashed line indicates mean fluorescence of *E. coli* cells harbouring the promoterless pUA66 plasmid as measured at 8 h.p.i. F, faeces. **b**, Competitive infection experiments. C.I. values for Δ*lsrB,* Δ*lsrC* and Δ*lsrD* in competitive infections against the WT strain. F, faeces, CC, caecal content. Lines indicate median values (minimum n=6, from at least two independent experiments). *P* values were

calculated using the Mann-Whitney test (***P<0.0005). **c**, Experimental scheme for competitive infection experiments with subsequent introduction of the AI-2- overproducing strain *E. coli* strain ARO071. SPF mice were pretreated with 20 mg ampicillin by oral gavage 24 h prior to inoculation with *E. coli* (1:1 mix WT vs Δ*lsrB*). At 48 h.p.i., mice were additionally inoculated with $5x10^7$ c.f.u. of *E. coli* ARO071 by oral gavage, resulting in increased luminal concentration of AI-2. **d**, C.I. values for Δ*lsrB* in Z1331 Δ*lsrB* vs WT *E. coli* Z1331 competitive infection before and after addition of the AI-2-overproducing *E. coli* ARO071. F, faeces, CC, caecal content. Lines indicate median values (n=6, from at least two independent experiments). *P* values were calculated using the Mann-Whitney test (**P*<0.05; ns, not significant). **e**, Competitive infection experiments of *E. coli* Z1331 vs *E. coli* 8178 (*lsr* operon-negative) or *E. coli* Z1331 Δ*lsrB* vs *E. coli* 8178. SPF mice were infected with *E. coli* Z1331 WT or Δ*lsrB* and *E. coli* 8178 WT ($5x10^7$ c.f.u. by gavage; 1:1000 ratio). F, faeces, CC, caecal content. Lines indicate median values (n=7, from at least two independent experiments). *P* values were calculated using the Mann-Whitney test (ns, not significant). **f**, Competitive infection experiments with or without AI-2 overproduction. SPF mice were infected with *E. coli* Z1331 WT or Δ*lsrB* and *E. coli* 8850 WT (*lsr* operon-positive; $5x10^7$ c.f.u. by gavage; 1:1000 ratio). To probe the effect of AI-2 overproduction, mice were inoculated with Z1331 vs 8850 as above, supplemented with *E. coli* ARO071 ($5x10^7$ c.f.u.; by gavage; at 1:1 ratio). F, faeces, CC, caecal content. Lines indicate median values (minimum n=6, from at least two independent experiments). *P* values were calculated using the Mann-Whitney test (****P*<0.0001; ****P*<0.0005; ***P*<0.005; **P*<0.05).

Genomic diversity of AI-2 sensing contributes to niche segregation of *E. coli* strains in the gut. The mammalian gut is a complex and dynamic environment with a fine scale spatial structure. Heterogenous spatial distribution of available nutrients, microorganisms, signalling and other host-derived molecules allows niche segregation and can thereby permit the stable co-existence of several strains of a given bacterial species based on their metabolic preferences[39–41]. The relevant metabolic pathways are thought to differ from case to case, and they were unknown for *E. coli* Z1331.

E. coli niche segregation was shown to depend at least partially on the differential ability of individual strains to utilize certain compounds as carbon or nitrogen source[42,43]. Intriguingly, the *lsr* operon (and thus the ability to sense and chemotactically respond to AI-2) is found in some, but absent in other *E. coli* strains[44]. We hypothesized that AI-2 sensing might contribute to niche segregation of *E. coli* strains in the gut. To test this, we analysed the competition of *E. coli* Z1331 against two other *E. coli* mouse isolates, *E. coli* 8178 which naturally lacks the *lsr*-operon and is therefore devoid of AI-2 signaling[45]; and *E. coli* 8850, which is naturally *lsr* positive[45]. The latter two strains were applied in a 1000-fold surplus (compared to *E. coli*

Z1331). The overabundance of *E. coli* 8178 or 8850 in the inoculum would allow these strains to rapidly occupy their respective niches. If chemotaxis towards AI-2 indeed allows *E. coli* Z1331 to reach a distinct niche and thus avoid direct competition with *E. coli* 8178, it should be able to grow up to reach a 1:1 ratio (at least in the absence of other competitive effects like bacteriocins production[46]). If true, *E. coli* Z1331 should not be able to catch up in growth with *lsr* positive *E. coli* 8850 strain. As seen in Fig. 2e and Extended Data Fig. 8d, *E. coli* Z1331 was indeed able to reach a 1:1 ratio compared to *E. coli* 8178 within 24 h.p.i. This phenotype was independent of LsrB, suggesting that *E. coli* Z1331 and 8178 do not compete for the LsrB-dependent niche. In this case, LsrB-dependent chemotaxis may therefore contribute to niche segregation in competitive infections.

In contrast, the *E. coli* 8850 outnumbered *E. coli* Z1331 by 10-50 fold throughout the course of the experiment (Fig. 2f). Deletion of *lsrB* further decreased fitness of Z1331 to 100-1000 fold, and this fitness defect was alleviated in presence of the AI-2-overproducing *E. coli* ARO071 (Fig. 2f and Extended Data Fig. 8e). As expected, no inflammation was observed upon infection of mice with *E. coli* 8178 and 8850 (Extended Data Fig. 8a-c). Additionally, colonization levels of *E. coli* 8850 remained unchanged in co-infection experiments with ARO071, suggesting that the regain of fitness by *E. coli* Z1331 Δ*lsrB* was not due to the competition between *E. coli* 8850 and ARO071 (Extended Data Fig. 8e). In agreement with this observation, the AI-2-deficient mutant of ARO071 was incapable of rescuing the *E. coli* Z1331 Δ*lsrB* phenotype (Fig. 2f). These findings suggest that the differential ability to sense and chemotactically respond to AI-2 can contribute to niche segregation of *lsr*-expressing and non-expressing *E. coli* strains in the gut.

***E. coli* Z1331 benefits from fructoselysine utilization in a LsrB-dependent manner.** Although degradation of AI-2 in *E. coli* cells yields acetyl-CoA and dihydroxyacetone phosphate, which in turn can be fed into glycolysis and the citric acid cycle[47], *E. coli* strains show generally poor or no growth with AI-2 as a sole carbon source[47,48]. Although the observed aggregation of *E. coli* Z1331 cells in the gut might be *per se* beneficial[14,49], we aimed at further deciphering how *E. coli* benefits from AI-2 chemotaxis *in vivo*. We reasoned that *lsr* positive *E. coli* strains, by reaching their respective ecological niche, might benefit from utilizing niche-specific nutrients. Therefore, we reasoned that the *lsr* operon may show a pattern of co-occurrence with genes responsible for the utilization of niche-specific nutrients when comparing *E. coli* genomes. To explore this, 10146 *E. coli* and *Shigella* genomes and their genes were downloaded from a high-quality genome collection[50]. In order to identify known genes and pathways that may be connected to the *lsr* operon, this collection was reprocessed to obtain gene frequencies of all genes with a known function in 47 different *E. coli* and *Shigella* lineages. The analysis resulted in a list of 168 genes whose presence correlated with *lsrB*

(Pearson correlation coefficient ≥0.5; Supplementary Table 2). These included structural, metabolic as well as regulatory genes and operons. Interestingly, among these correlated genes were those belonging to the *frl* operon, which is required for fructoselysine utilization[51]. Fructoselysine, an Amadori product of the non-enzymatic reaction of glucose with primary amines, is highly abundant in thermally processed foods including mouse chow[52,53].

We compared the phylogenetic relatedness, measured by extracting the tree branch length from a maximum likelihood phylogenetic tree of representative genomes, as well as the functional similarity, based on the fraction of shared annotated genes with a known function, of all 47 lineages in an all-against-all manner. In addition to the previously observed correlation of *lsrB* and *frlA* genes, we could thereby show that lineages which possess both *lsrB* and *frlA* are closely related to one another, both in evolutionary distance as well as functional similarity. When comparing these lineages to others which encode neither of the two genes, the opposite trend was apparent, e.g., they were considerably more dissimilar in the phylogenetic relatedness and functional similarity (Fig. 3a, Extended Data Fig. 9). Consistent with a role in gut colonization by particular *E. coli* strains, mutations in the *frl* operon repressor FrlR were detected in long-term colonization experiments with an *frl*-positive *E. coli* strain[54,55]. Accordingly, the deletion of the *frl* operon attenuated *E. coli* Z1331 gut luminal growth in competitive infection experiments (Fig. 3b). In order to assess if fructoselysine utilization requires LsrB-dependent chemotaxis, we created an equivalent pair of isogenic mutants in a *lsrB*-deficient background. In competitive infections, *E. coli* Z1331 Δ*lsrB* Δ*frl* colonized the gut as well as *E. coli* Z1331 Δ*lsrB* (C.I.≈1; Fig. 3b). Moreover, increasing the luminal AI-2 levels using *E. coli* ARO071 abolished the fitness advantage of the WT *E. coli* Z1331 over *E. coli* Z1331 Δ*frl*, suggesting a direct connection between AI-2 chemotaxis and fructoselysine utilization (C.I.≈1; Fig. 3b). We therefore conclude that *E. coli* Z1331 requires *lsrB* in order to benefit from fructoselysine. We further selected and tested several other genes from the Supplementary Table 2, but failed to identify those potentially connected to AI-2 chemotaxis (Supplementary Table 3).

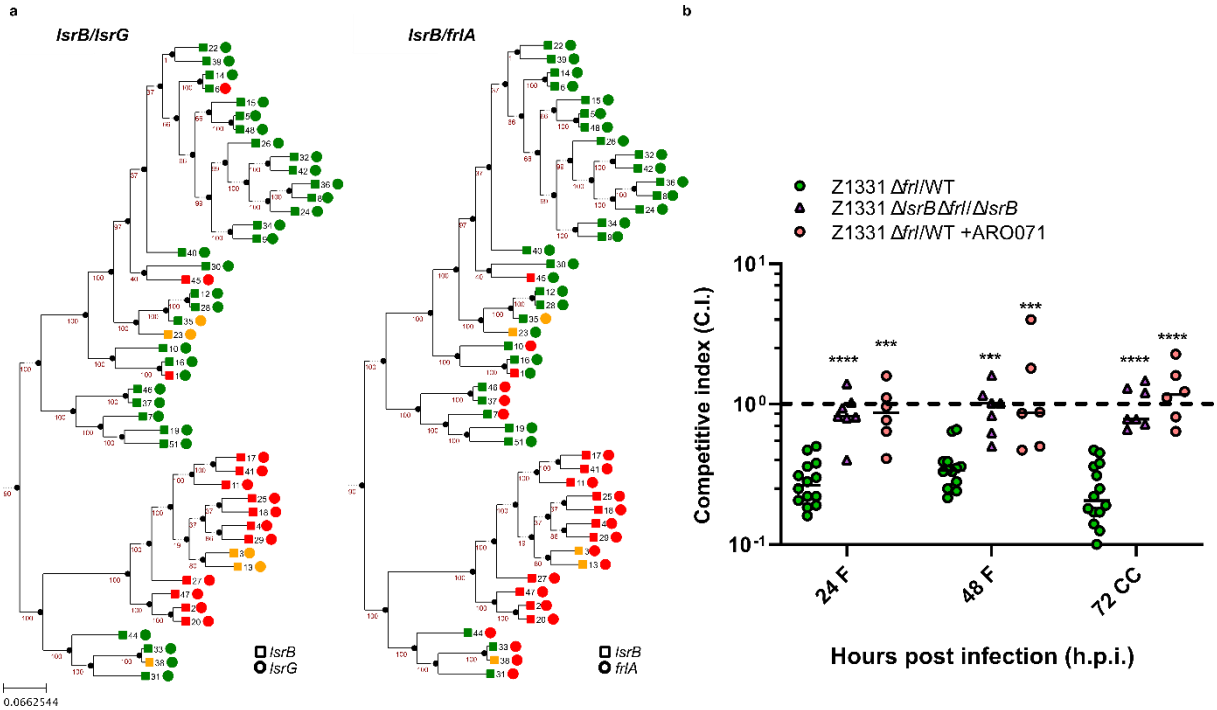

Figure 3. Co-occurrence analysis and competitive infection experiments demonstrating a functional link between fructoselysine utilization and LsrB in *E. coli* Z1331. a, Maximum likelihood phylogenetic tree of representative genomes from the 47 investigated *E. coli* lineages. We annotated with the gene frequencies of *lsrB* and *lsrG* (positive control) and for *frlA* and *lsrB* genes. Bootstrap values are shown in red. A green dot indicates the respective gene is present in the majority of genomes belonging to the respective lineage (>95% of all genomes possess the gene), orange means partly present (5%-95%) and red means it is not present (<5%). **b,** C.I. values for *E. coli* Z1331 Δ*frl* knockout during competitive infection against the WT strain in the WT and the Δ*lsrB* strain background in the absence or the presence of the AI-2 overproducing *E. coli* strain ARO071. F, faeces, CC, caecal content. Lines indicate median values (minimum n=6, from at least two independent experiments). *P* values were calculated using Mann-Whitney test (****$P<0.0001$; ***$P<0.0005$).

Fructoselysine is an attractant sensed by the chemoreceptor Trg. To further investigate the interplay between AI-2 chemotaxis and fructoselysine metabolism, we analysed the chemotactic response of *E. coli* to fructoselysine using a well-established Förster resonance energy transfer (FRET) assay[56]. This assay allows investigating the response of the chemotaxis pathway to its ligands by monitoring the phosphorylation-dependent interaction between fluorescent CheY-YFP and CheZ-CFP fusion proteins[57,58]. Since the chemotaxis signalling pathway is highly conserved between different *E. coli* strains, the FRET assay could be performed in the *E. coli* K-12 derivative strain W3110. As wild type *E. coli* isolates like those employed in our study do often fail to express motility and chemotaxis genes under the FRET assay conditions[59], we have used *E. coli* W3110 for FRET experiments. In the wild-type *E. coli*

K12 cells, we observed an attractant response to 1-30 µM fructoselysine, as reflected by the rapid drop in the YFP/CFP fluorescence ratio. (Fig. 4a, b, Extended Data Fig. 10a). *E. coli* strains typically possess up to 5 different types of chemoreceptors responsible for sensing a large repertoire of molecules[1]. To pinpoint the chemoreceptor involved in the chemotactic response to fructoselysine, we performed FRET assays using *E. coli* K12 strains deleted for each of the four receptors (Tar, Tsr, Trg and Tap) that mediate responses to chemical ligands. The response to fructoselysine was severely reduced in Δ*trg* knockout cells, suggesting that chemotaxis to fructoselysine is mediated by Trg (Fig. 4a, b, Extended Data Fig. 10b). In contrast, a specific response to fructoselysine was retained in the knockouts of *ptsI* (phosphotransferase enzyme of the phosphotransferase system which is involved in chemotactic response to some sugars[60]) and other receptor genes (Fig. 4a, Extended Data Fig. 10c-g), including the AI-2-specific receptor Tsr and also dipeptide receptor Tap that showed genome correlation with *lsr* operon (Extended Data Fig. 10e, Supplementary Table 2).

However, although Trg-mediated chemotaxis apparently represents the primary mechanism of cell attraction towards fructoselysine, no effect of Δ*trg* deletion in *E. coli* Z1331 was observed in *in vivo* experiments (Fig 4c). This might be due to the pleiotropic nature of the Δ*trg* deletion, since Trg is known to mediate chemotactic responses to several sugars[61], which may have different effects on the cell fitness in the gut context. A similar situation was observed for strain lacking Tsr, that mediates the response to AI-2 but also to a number of other stimuli, including amino acids, pH and redox potential[61]. Despite sharing the same signalling pathway of AI-2 sensing, Δ*lsrB* and Δ*tsr* strains show opposite competitive indexes in mouse experiments (Fig. 2b, Extended Data Fig. 11), again likely due to the impact of the Δ*tsr* deletion on responses other than AI-2. Further studies are needed to understand this complexity.

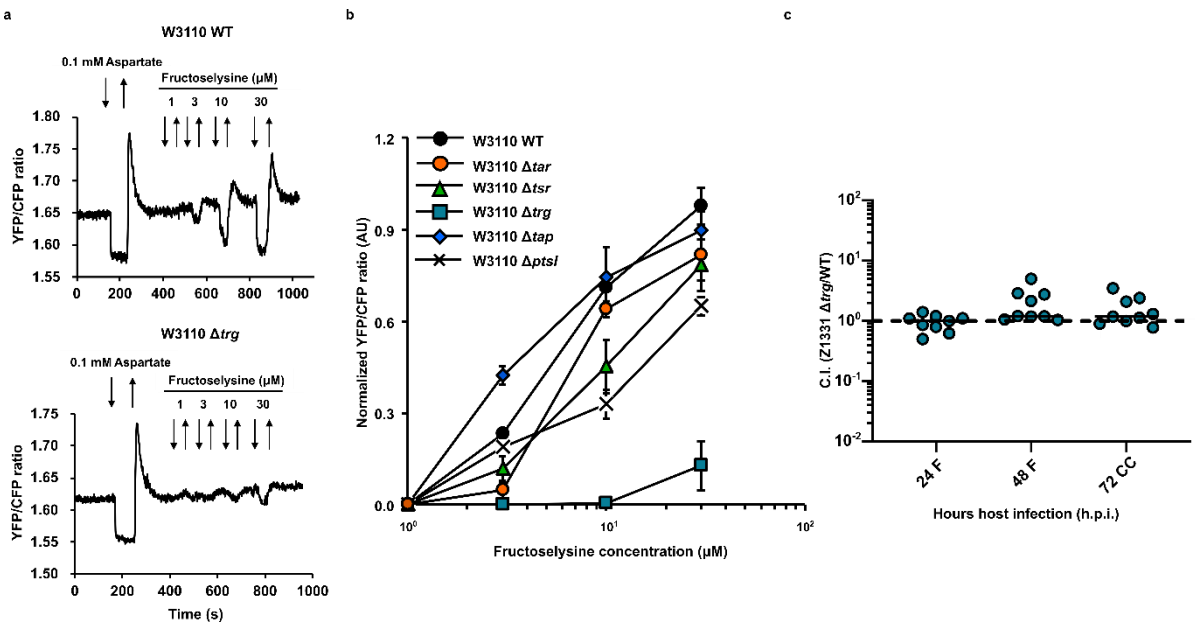

Figure 4. Fructoselysine is an attractant sensed by Trg chemoreceptor. a, Examples of FRET measurements of *E. coli* W3110 wild-type and Δ*trg* responses to fructoselysine. The efficiency of FRET and thus the activity of chemotaxis pathway is reflected by the ratio of YFP/CFP fluorescence. Stimulation with an attractant results in pathway inactivation and thus decrease in the FRET ratio. Buffer-adapted cells were stimulated with step-like addition and subsequent removal of compounds, indicated by downward and upward arrows, respectively. Stimulation with a saturating concentration of strong attractant aspartate was used as a positive control. **b,** Dose-response curves of *E. coli* W3110 wild-type, chemoreceptor (Δ*tar*, Δ*tsr*, Δ*trg*, Δ*tap*) and PTS (Δ*ptsI*) knockout strains to fructoselysine. Means of three independent values of the pathway response upon step-like stimulation with indicated concentrations of fructoselysine measured by FRET as in (a) and in Extended Data Fig. 10, normalized to the maximal response to control attractants aspartate or serine are shown. Direct effect of fructoselysine on the YFP/CFP fluorescence ratio, measured in the negative control strain, was subtracted. Error bars indicate s.d.. **c**, Competitive infection experiment. C.I. values for *E. coli* Z1331 Δ*trg* knockout during competitive infection against the WT strain. F, faeces, CC, caecal content. Lines indicate median values (n=9, from at least two independent experiments).

Fructoselysine utilization represses *lsr* operon expression, resulting in accumulation of extracellular AI-2. Since the chemotactic responses to fructoselysine and AI-2 are directly related, we further aimed at understanding the connection between self-produced AI-2 and fructoselysine metabolism. We hypothesized that fructoselysine uptake and metabolism might affect *lsr* operon activity. Addition of 1% fructoselysine to exponentially growing *E. coli* Z1331 cultures resulted in decreased *lsr* operon expression, and the observed inhibition was independent of fructoselysine (Δ*frlA*) or AI-2 (Δ*lsrB*) import (Fig. 5a). Interestingly, no repression of *lsr* operon activity was detected in a phosphotransferase system (PTS)-deficient Δ*ptsI* knockout strain, albeit at reduced background levels of *lsr* expression. *lsr* operon expression is known to be regulated by catabolite repression, resulting in inhibition of its expression upon import of sugars through the PTS mediated by cAMP and its receptor CRP[62,63]. This suggests that although the *frl* operon encodes a fructoselysine importer[51], fructoselysine might be partially imported via PTS or its uptake affects the activity of PTS indirectly, similar to several other non-sugar carbon sources (Extended Data Fig. 12)[60]. Indeed, de-repression of *frl* operon expression caused by FrlR inactivation upon addition of fructoselysine[64] was only detected in Δ*ptsI* background (Fig. 5b). This suggests a rather unconventional double regulation of the *frl* operon activity by fructoselysine interactions with PTS and FrlR. Consistent with CRP-mediated regulation of *frl* operon activity, we observed a decreased *frlA* promoter activity in presence of glucose, a known PTS substrate, and

fructoselysine in both WT and fructoselysine import-deficient Δ*frlA* strains[64]. At this point, further studies are needed to clarify the mode of interaction between fructoselysine and PTS. Apart from CRP-mediated catabolite repression of the *frl* operon, direct inhibition of fructoselysine kinase FrlR by the unphosphorylated form of the PTS phosphocarrier protein HPr might as well be possible. This has been previously shown for the *lsr* operon, where unphosphorylated HPr inhibited AI-2 kinase LsrK[63].

Upon its activation, the *lsr* operon induces rapid import and degradation of extracellular AI-2[34]. Decreased *lsr* operon activity as a response to fructoselysine metabolism might result in increased extracellular AI-2 levels. To test this hypothesis, we incubated *E. coli* Z1331 cells with or without 1% fructoselysine, followed by measurements of extracellular AI-2. As expected, fructoselysine-dependent inhibition of *lsr* operon activity resulted in elevated extracellular AI-2 levels (Fig. 5c). By generating more AI-2, fructoselysine-metabolizing *E. coli* might thus recruit additional cells to the source of fructoselysine in the gut.

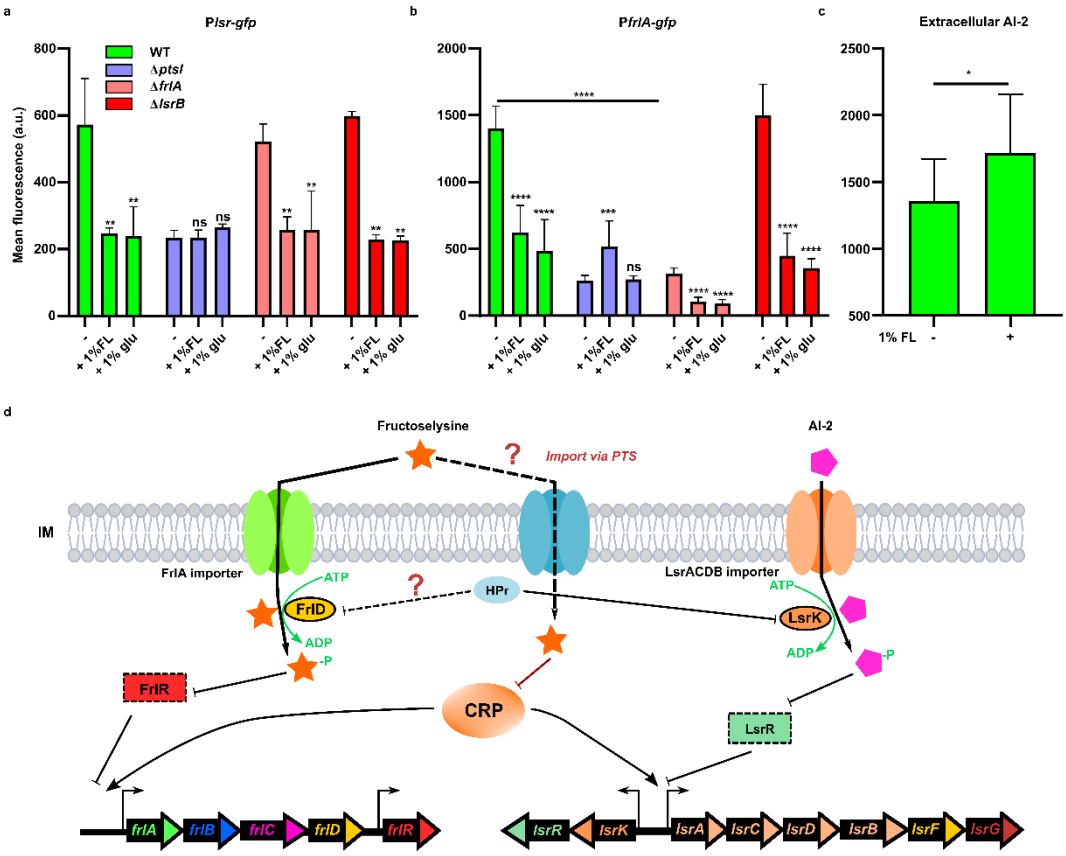

Figure 5. Effect of fructoselysine on *lsr* and *frl* operon expression in *E. coli* Z1331. a, *lsr* and **b**, *frl* operon activity in absence and presence of 1% fructoselysine (FL) in *E. coli* WT and its PTS-, fructoselysine and AI-2 import-deficient knockouts (Δ*ptsI*, Δ*frlA* and Δ*lsrB,* respectively). FL was added to exponentially growing *E. coli* cells (TB medium) containing

plasmid based P*lsr-gfp* or P*frlA-gfp* fluorescent reporter. Glucose (glu), was used as a positive control for PTS system effects. Fluorescence was measured 2 h after incubation with FL or glucose with flow cytometry and expressed in arbitrary units (a.u.). Error bars indicate s.d. (n=6, from at least two independent experiments). **c**, Levels of extracellular AI-2 produced by *E. coli* cells quantified in supernatants using fluorescence reporter strains as described in Methods. Reporter fluorescence was measured with flow cytometry and expressed in arbitrary units (a.u.). Error bars indicate s.d. (minimum n=7, from at least two independent experiments). *P* values were calculated using the Mann-Whitney test $^{**}P<0.005$; $^{*}P<0.05$; ns, not significant). **d**, Working model of FL- and AI-2-mediated regulation of *frl* and *lsr* operons, respectively. Import of AI-2 via the LsrACDB importer results in de-repression of the *lsr* operon. Note that AI-2 internalization in *E. coli* is not solely dependent on the Lsr system[34,65]. Our data indicates that FL appears to interact with a PTS system (dashed line, is potentially imported via an unidentified PTS), leading to catabolite repression of both *frl* and *lsr* operons via CRP. In case of the *frl* operon, FrlA-mediated FL import can slightly upregulate transcription, presumably by alleviating FrlR-mediated repression (that is induction; as seen in the *ptsI* mutant). *frl* operon repression by PTS might however also occur via direct inhibition of the fructoselysine kinase FrlD by the PTS phosphocarrier protein HPr (dashed line), as previously shown for the *lsr* operon. Fructoselysine-dependent inhibition of *lsr* operon expression results in less AI-2 import and therefore higher levels of extracellular AI-2, as seen in panel c. IM, inner membrane. Question marks indicated potential interactions that are yet to be experimentally addressed.

Discussion

Chemotactic bacteria are found in various environments, ranging from the rhizosphere and aquatic habitats to the mammalian gut. The role of chemotaxis in nutrient acquisition, biofilm formation and host-microbe interactions has been clearly shown for several bacterial species[8]. However, despite our detailed knowledge of its underlying molecular machinery, the importance of chemotactic behaviour in bacteria under physiologically relevant conditions remains poorly studied[9]. *E. coli*, a common mammalian gut inhabitant, has been shown to benefit from chemotaxis on both individual and population levels. In a series of *in vitro* studies, the role of chemotaxis in its foraging behaviour, expansion of the population range, autoaggregation and biofilm formation has been well documented[13–15,66–68]. Surprisingly, although *E. coli* has been a preferred model for *ex vivo* chemotaxis studies for decades, the question of how it might benefit from chemotaxis *in vivo* has not yet been fully addressed. In this study, we combined molecular and bioinformatics approaches to understand the role of *E. coli* chemotaxis system during gut colonization.

By competing the non-chemotactic Δ*cheY* knockout against the WT strain in ampicillin-pretreated SPF mice, we could clearly show the fitness advantage of chemotaxis for *E. coli*

Z1331 *in vivo*. Interestingly, although a similar phenotype was previously observed for Δ*cheY* mutants during *S.* Tm infection, this latter phenotype was strongly associated with gut inflammation[30]. In contrast, no inflammation was observed during our colonization experiments with *E. coli*, suggesting that even in closely related enteric organisms like *E. coli* and *S.* Tm, chemotaxis can be adopted for different strategies of proliferation and survival in the gut environment. It is important to note that *E. coli* is as well capable of adapting another strategy during gut colonization, namely inactivating motility and chemotaxis. Building and maintaining motility and chemotaxis machinery represents one of the most energetically costly behaviours for the cell[1,2], and mutations that inhibit flagella synthesis might prove beneficial under certain conditions. However, our data suggests that chemotaxis indeed provides fitness advantages for motile *E. coli* strains across different phylogroups[12,69–71].

We further show that the fitness advantage provided by chemotaxis is largely dependent on the response to the self-produced interspecies quorum sensing signal AI-2. Multiple roles of AI-2 signalling in collective behaviour of bacteria, phage-bacteria interactions and gut community structure have been reported[16,21,48,72]. Chemotaxis towards AI-2 promotes autoaggregation and biofilm formation in *E. coli* and biofilm dispersal in *Helicobacter pylori*[14,15,73,74]. Moreover, the chemotactic response to AI-2 is apparently not limited to AI-2 producing bacteria, suggesting its broad function in host-associated communities[19].

In *E. coli*, AI-2 is indirectly sensed by the Tsr chemoreceptor via AI-2 binding LsrB protein[36]. LsrB is in turn encoded by the AI-2-responsive *lsr* operon required for rapid signal internalization and degradation[16]. The ability of an *E. coli* strain to chemotactically respond to AI-2 is thus tightly linked to the presence of the *lsr* operon, which may be different in other bacteria[44]. One of the competitive fitness advantages provided by AI-2 in the gut is related to the niche segregation between *E. coli* strains that differ in their ability to chemotactically respond to AI-2. Given that any gut ecosystem might contain several strains of the same bacterial species that must stably coexist over extended period of time[39–41], their segregation due to different tactic preferences might generally facilitate such co-existence, either on its own or in combination with different metabolic preferences or utilization of the same nutrients in distinct niches (niche segregation) as proposed by a niche theory[41,75]. The former case might apply to AI-2, since it is not directly used by *E. coli* as a nutrient source[47,48], thus expanding the nutrient niche theory to molecules with no apparent nutritional value.

The inability of *E. coli* to use AI-2 as sole nutrient, however, poses a question of how exactly *E. coli* benefits from AI-2 chemotaxis during gut colonization. To address this question, we analysed 10146 *E. coli* and *Shigella* genomes to find genes correlated with the presence of the *lsr* operon. We found some level of correlation between *lsr* and the *frl* operon, which is required for fructoselysine utilization. This is of particular interest, since fructoselysine is widely found in thermally processed foods[53]. Indeed, we could show that *E. coli* cells benefit from

fructoselysine utilization in a AI-2 chemotaxis-dependent manner. Intriguingly, although our experiments revealed that fructoselysine could itself act as an attractant sensed via the chemoreceptor Trg, its primary mode of signalling might rather rely on the regulation of local AI-2 levels in the gut, mediated by the inhibitory effect of fructoselysine on *lsr* operon expression and therefore leading to increased extracellular AI-2 levels. We hypothesize that fructoselysine chemotaxis and metabolism, by increasing AI-2 levels surrounding fructoselysine-utilizing cells, attracts AI-2 chemotactic *E. coli* to the source of fructoselysine. Consistently, a positive loop in AI-2-mediated cell recruitment was previously reported for growing aggregates of *E. coli* cells *in vitro*[14]. Furthermore, it has been proposed that such integration of two independent signalling pathways enhances chemotaxis of *E. coli* cells towards the nutrient source[76].

AI-2 is produced and sensed by a wide range of bacterial species, with AI-2 mimics being synthesized by eukaryotic cells[16–18]. Given the apparently ubiquitous presence of this signal, it seems rather counter-intuitive that *E. coli* cells rely on it to occupy specific niche within the gut. A possible explanation for that would be that AI-2 chemotaxis is only relevant under antibiotics- or inflammation-induced dysbiosis conditions, which are known to result in microbiota suppression and expansion of Enterobacteriaceae[77–80]. In absence of other AI-2 producers, no interference with self-produced AI-2 would occur. Additionally, our analysis shows that *E. coli* lineages that possess both *lsr* and *frl* operons show high levels of similarity to each other both in terms of their phylogenetic relatedness as well as in their functional potential, ensuring that closely related *E. coli* have higher chances of co-accumulation at the fructoselysine source than more distantly related strains. Collectively, our study provides first evidence for a causal link between AI-2 chemotaxis, gut colonization and niche segregation of *E. coli* strains in the mammalian gut. It further establishes a link between AI-2 chemotaxis and fructoselysine metabolism *in vivo*. We suggest that similar mechanisms of AI-2-mediated host colonization might exist in other chemotactic bacteria.

Materials and Methods

Bacterial strains and growth conditions

The strains and plasmids used in this study are listed in Supplementary table 1. *E. coli* cells were routinely grown either on 1.5% Lysogeny Broth (LB) agar or in liquid LB or tryptone broth (TB) medium (10 g tryptone, 5 g NaCl per litre) supplemented with ampicillin (100 µg/ml), kanamycin (50 µg/ml), streptomycin (50 µg/ml) or chloramphenicol (35 µg/ml), where necessary. For fructoselysine utilization experiments, M9 minimal medium (6.7 g Na_2HPO_4, 3 g KH_2PO_4, 0.5 g NaCl, 1 g NH_4Cl per litre, 2 mM $MgSO_4$, 0.1 mM $CaCl_2$) was used. Gene

deletions were obtained via PCR-based inactivation[81], and Km^r cassettes were eliminated via FLP recombination[82].

Animals

C57BL/6 (JAX:000664, The Jackson Laboratory) mice were held under specific pathogen-free (SPF) conditions at the EPIC facility at ETH Zürich. Germ-free (GF) mice were bred in flexible film isolators at the isolator facility (EPIC, ETH Zürich). All animal experiments were reviewed and approved by Kantonales Veterinäramt Zürich under license ZH158/2019, complying with the cantonal and Swiss legislation. 8-12 week old mice of both sexes were randomly assigned to experimental groups.

Mouse infection experiments

8-12 week old SPF mice were orally pretreated with ampicillin (20 mg) 24 h prior infection. No pretreatment was required prior to infection of GF mice. *E. coli* cultures were grown overnight in TB at 37 ˚C with shaking, diluted 1:100 in fresh TB and incubated at 37 ˚C with shaking to the OD_{600}=0.5-0.6 was reached. The cells were then washed in PBS (137 mM NaCl, 2.7 mM KCl, 10 mM Na_2HPO_4, 1.8 mM KH_2PO_4), and mice were orally gavaged with $5x10^7$ c.f.u. in 50 µl of single culture or a 1:1 mixture of strains, unless specified otherwise. Faecal samples were collected every 24 h, unless stated otherwise, and animals were sacrificed at 72 or 96 h.p.i. by CO_2 asphyxiation. Fresh faecal pellets and intestinal contents were harvested and suspended in 500 µl PBS, followed by homogenization in a Tissue Lyser (Qiagen). Bacteria were plated on MacConkey (Oxoid) or LB agar plates with appropriate antibiotics.

Competitive index (C.I.) of a wild-type strain (WT) and respective knockouts (KO) in a competitive infection was determined as a ratio between c.f.u. (KO) and c.f.u. (WT) divided by the ratio of both strains in the inoculum. In most cases, competitive infection assays can resolve gut lumen colonization phenotypes of Enterobacteriaceae much better than a comparison between data from animals that are infected with either the wild-type or the mutant strain alone. This is likely attributable to the fact that these Enterobacteriaceae strains generally do not reach their fastest possible growth rate in the gut lumen, at least in the absence of massive bacteriotoxic events (like massive gut inflammation). Thus, slightly reduced efficiency of one mechanism to access a particular fraction of the nutrients can be compensated by utilizing alternative, even if less efficient, mechanisms. As a result, competitive infection assays in the non-inflamed gut are not accompanied by a significant change in the overall *E. coli* density, while competitions between a wild-type strain and an attenuated mutant would still yield a significant competitive index.

Immunofluorescence microscopy and image analysis

SPF ampicillin-pretreated mice were infected with $5x10^7$ c.f.u. (single infection or 1:1 mix) of *E. coli* Z1331 WT and Δ*cheY* carrying pFPV25.5 (mCherry under control of constitutive *rpsM* promoter) and pFPV25.1 (GFP under control of constitutive *rpsM* promoter) plasmids, respectively[83,84]. At 72 h.p.i., mice were sacrificed by CO_2 asphyxiation. Caecal contents were collected and plated to confirm the expected C.I. (Δ*cheY*/WT). Small intestine (Ileum), caecal and proximal colon tissue was excised, fixed in 4% paraformaldehyde (w/v in PBS) for 48 h at 4 ˚C, followed by 4 h in 20% sucrose solution (w/v in PBS) at 4 ˚C. The samples were then embedded and frozen in Tissue-Tek OCT medium (Sysmex). 10 µm sections of the resulting cryoblocks were cut and stained using DAPI and Cy5-Phalloidin. Images of fixed tissues were visualized using a confocal Zeiss Axiovert 200 m microscope equipped with two evolve 512 EMCCD cameras (Photometrics) and a 40x oil objective. Images were analysed using Particles Analysis Tool (ImageJ, https://imagej.nih.gov/) to determine the number of aggregated formed by WT and Δ*cheY* cells. Aggregates were defined as objects with the size at least 50 px^2, with single cells being ~10 px^2. The number of aggregates formed by WT and Δ*cheY* cells was then normalized to the total amount of detected particles in mCherry and GFP channels. Fluorescent particles of non-bacterial origin (i.e., food particles) were manually excluded from the analysis.

Flow cytometry

Activity of the *lsr* promoter was analyzed *in vivo* in SPF ampicillin-pretreated mice using a plasmid-based P*lsr-gfp* reporter[14]. Fresh faecal pellets were collected at 8, 24 and 48 h.p.i., incubated for 1 h at room temperature with 2 µg/ml chloramphenicol to inhibit protein synthesis and to allow GFP proteins to fully maturate. Maximum of 20% reporter plasmid loss was observed during the experiment as determined by differential plating of faeces. Fluorescence was measured with Cytoflex flow cytometer (Beckman Coulter). *In vitro* culture of *E. coli* cells was used as a control for a forward and side scatter gate to exclude debris.

Extracellular AI-2 measurements

Extracellular AI-2 in faeces was measured by the same plasmid-based P*lsr-gfp* reporter introduced into *E. coli* W3110 Δ*luxS* strain[14]. Faecal suspensions were centrifuged for 10 min at 14 000 r. p.m. 20 µl aliquots of the reporter strain (OD_{600}=0.3-0.5) were added to debris-free supernatants. Fluorescence of the reporter was measured after 1 h of incubation at 37 ˚C with shaking.

To measure AI-2 levels in *E. coli* supernatants treated with fructoselysine, exponentially growing *E. coli* Z1331 cells were incubated for 2 h with or without 1% fructoselysine. The cells

were subsequently washed twice in PBS and incubated for additional hour in fresh TB to allow for AI-2 production. AI-2 levels in cell-free supernatants were measured as described above.

Lipocalin-2 ELISA

Lipocalin-2 was measured in faeces and caecal contents homogenized in 500 µl PBS by ELISA DuoSet Lipocalin ELISA kit (DY1857, R&D Systems).

Histopathology

Caecal tissue samples were embedded and frozen in Tissue-Tek OCT medium (Sysmex). Cryosections (10 µm) were stained with haematoxylin and eosin (H&E). Pathological analysis (submucosal edema, goblet cells numbers, epithelial integrity and polymorphonuclear granulocytes infiltration into the lamina propria) was performed as described previously[85].

Fructoselysine synthesis

Fructoselysine synthesis was performed as previously described[86].

FRET measurements

The FRET measurements were performed as previously described[57,58]. Briefly, *E. coli* cells were grown in TB supplemented with the antibiotics (100 mg/mL ampicillin) and inducer (50 mM IPTG) at 34 °C and 275 r.p.m. Cells were harvested at OD_{600}=0.6 by centrifugation (4000 r.p.m. for 5 min), washed twice with tethering buffer (10 mM KPO_4, 0.1 mM EDTA, 1 µM methionine, 10 mM lactic acid, pH 7), and stored at 4 °C for 30 min. The sample was attached to a polylysine-coated coverslip, placed in a flow chamber under constant flow (300 µl/min) of tethering buffer using a syringe pump (Harvard Apparatus, Massachusetts, United States), which was used for stimulation with compounds of interest. Measurements were performed on an upright fluorescence microscope (Zeiss AxioImager.Z1) equipped with photon counters (Hamamatsu) connected to a computer with custom written LabView7 software (National Instruments). CFP fluorescence was excited at 436/20 nm through a 455 nm dichroic mirror by a 75 W Xenon lamp. To detect CFP and YFP emissions, 480/40 nm band pass and 520 nm long pass emission filters were used, respectively. Fluorescence of a monolayer of 300–500 cells was continuously recorded in the cyan and yellow channels using photon counters with a 1.0 s integration time.

Bioinformatic analysis

The genome collection provided by Horesh *et al*. was used as a base for our bioinformatic analysis[50]. Briefly summarizing their work, the authors downloaded 18156 *E. coli*

and *Shigella* genomes from human hosts and extensively curated them, resulting in a high-quality dataset of 10146 genomes. Coding sequences were identified with Prodigal[87] and annotated with PROKKA[88] and genomes were assigned to lineages with a k-mer based whole-genome comparison approach using popPUNK[89].

We downloaded the supplementary files from the publicly available collection (https://microbiology.figshare.com/articles/dataset/A_comprehensive_and_high-quality_collection_of_E_coli_genomes_and_their_genes/13270073, assessed on 16.08.2021) and used the Supplementary file F4 to obtain gene annotations and lineage assignments for each genome. Selected annotations of interest, such as the *lsr* operon and associated genes, were manually verified by blasting the representative sequence with blastx[90]. We excluded the gene family "*lsrB*_1", which mapped best to "*LacI* family transcriptional regulator [*Escherichia coli*]", hence most likely not corresponding to a functional *lsrB* protein. Some gene clusters encoding the same function were split up in the original analysis, for example *frlA*_1 and *frlA*_2. We used the short names to merge gene clusters with the same known function in every genome with a custom script in Python 3.7.6., generating a presence/absence matrix resulting in a total amount of 3964 annotated genes (https://github.com/lukasmalfi/E_Coli). This matrix was combined with the lineage assignment of each genome to compute gene frequencies (percentage of genomes within one lineage in which the respective gene is present) for all lineages containing >20 genomes, dividing the sum of genomes encoding a respective gene by the total amount of genomes. This process was repeated for each gene and lineage, resulting in a gene frequency table of all 47 lineages and 3964 genes.

Pearson correlation values of the *lsrB* frequencies against all other gene frequencies were computed from the gene frequency table using the DataFrame.corr function of pandas 1.0.3[91]. The resulting coefficients were sorted in descending order and descriptions for gene short names were obtained from the *E. coli* K12 MG1655 genome in the STRING Database Version 11.5[92].

The maximum likelihood phylogenetic tree "tree_50.nwk", based on single nucleotide polymorphisms in the core-gene alignment of one representative genome per lineage, was obtained from the previously mentioned data collection and edited using the ete3 toolkit version 3.1.2[93]. The representative genomes were chosen in the genome collection by Horesh et al., with Treemer v 3.0 to ensure a sub-sample that is representative of the original diversity[94]. We subsequently removed the three lineages (21,43,49) that contained less than 20 genomes from the tree and colored the nodes of the remaining lineages according to the gene frequencies of both *lsrB* and *frlA*, as well as *lsrB* and *lsrG* to serve as a positive control.

To compare the similarity of lineages containing both *lsrB* and *frlA* in comparison to lineages that possess only one or none of the genes of interest, we used two parameters, their

evolutionary distance and their functional similarity. When comparing two lineages, the tree branch length extracted from the phylogenetic tree with the get_distance function of the ete3 toolkit version 3.1.2 was used as a proxy for their evolutionary distance. To obtain a value for the functional similarity of two lineages, the fraction of shared annotated gene frequencies was calculated. For each gene with a known function, the lower frequency was identified, and the sum of all lower frequencies was divided by the sum of all higher frequencies, resulting in a value ranging from 1 (all gene frequencies are exactly the same in both lineages) to 0 (none of the genes are present in both lineages). This was done using the NumPy package version 1.18.1[95].

All lineages (n=47) were assigned into one of three groups: Containing both lsrB as well as frlA (gene frequency of both genes >0.1, n=24), containing neither of the two genes (gene frequency of both genes <0.1, n=13) or containing only one of the two genes (n=10). All lineages were then compared with one another and a scatter plot illustrating the comparison of functional and genomic relatedness of all lineages, colored according to their assignment to the three groups, was generated with bokeh version 2.2.3 (https://bokeh.org/).

References

1. Colin, R., Sourjik, V. & R Colin, V. S. Emergent properties of bacterial chemotaxis pathway. **39**, 24–33 (2017).

2. Milo, R., Jorgensen, P., Moran, U., Weber, G. & Springer, M. BioNumbers--the database of key numbers in molecular and cell biology. *Nucleic Acids Res.* **38**, (2010).

3. Ni, B., Colin, R., Link, H., Endres, R. G. & Sourjik, V. Growth-rate dependent resource investment in bacterial motile behavior quantitatively follows potential benefit of chemotaxis. *Proc. Natl. Acad. Sci. U. S. A.* **117**, 595–601 (2020).

4. Matilla, M. A. & Krell, T. The effect of bacterial chemotaxis on host infection and pathogenicity. *FEMS Microbiol. Rev.* **42**, 40–67 (2018).

5. Matilla, M. A. *et al.* Chemotaxis of the Human Pathogen Pseudomonas aeruginosa to the Neurotransmitter Acetylcholine. *MBio* (2022) doi:10.1128/MBIO.03458-21.

6. Lopes, J. G. & Sourjik, V. Chemotaxis of Escherichia coli to major hormones and polyamines present in human gut. *ISME J.* **12**, 2736 (2018).

7. Yang, J. *et al.* Biphasic chemotaxis of Escherichia coli to the microbiota metabolite indole. *Proc. Natl. Acad. Sci. U. S. A.* **117**, 6114–6120 (2020).

8. Colin, R., Ni, B., Laganenka, L. & Sourjik, V. Multiple functions of flagellar motility and chemotaxis in bacterial physiology. *FEMS Microbiol. Rev.* **45**, 1–19 (2021).

9. Keegstra, J. M., Carrara, F. & Stocker, R. The ecological roles of bacterial chemotaxis. *Nat. Rev. Microbiol. 2022* 1–14 (2022) doi:10.1038/s41579-022-00709-w.

10. Liou, M. J. *et al.* Host cells subdivide nutrient niches into discrete biogeographical microhabitats for gut microbes. *Cell Host Microbe* (2022) doi:10.1016/J.CHOM.2022.04.012.

11. McCormick, B. A., Laux, D. C. & Cohen, P. S. Neither motility nor chemotaxis plays a role in the ability of Escherichia coli F-18 to colonize the streptomycin-treated mouse large intestine. *Infect. Immun.* **58**, 2957 (1990).

12. Leatham, M. P. *et al.* Mouse intestine selects nonmotile flhDC mutants of Escherichia coli MG1655 with increased colonizing ability and better utilization of carbon sources. *Infect. Immun.* **73**, 8039–8049 (2005).

13. Song, S. & Wood, T. K. The Primary Physiological Roles of Autoinducer 2 in Escherichia coli Are Chemotaxis and Biofilm Formation. *Microorg. 2021, Vol. 9, Page 386* **9**, 386 (2021).

14. Laganenka, L., Colin, R. & Sourjik, V. Chemotaxis towards autoinducer 2 mediates autoaggregation in Escherichia coli. *Nat. co* **7**, 12984 (2016).

15. Jani, S., Seely, A. L., Peabody V, G. L., Jayaraman, A. & Manson, M. D. Chemotaxis to self-generated AI-2 promotes biofilm formation in Escherichia coli. *Microbiology* (2017) doi:10.1099/mic.0.000567.

16. Pereira, C. S., Thompson, J. a. & Xavier, K. B. AI-2-mediated signalling in bacteria. *FEMS Microbiol. Rev.* **37**, 156–181 (2013).

17. Ismail, A. S., Valastyan, J. S. & Bassler, B. L. A Host-Produced Autoinducer-2 Mimic Activates Bacterial Quorum Sensing. *Cell Host Microbe* **19**, 470–480 (2016).

18. Valastyan, J. S., Kraml, C. M., Pelczer, I., Ferrante, T. & Bassler, B. L. Saccharomyces cerevisiae requires cff1 to produce 4-hydroxy-5-methylfuran-3(2h)-one, a mimic of the bacterial quorum-sensing autoinducer ai-2. *MBio* **12**, 1–17 (2021).

19. Zhang, L. *et al.* Sensing of autoinducer-2 by functionally distinct receptors in prokaryotes. *Nat. Commun. 2020 111* **11**, 1–13 (2020).

20. Laganenka, L. & Sourjik, V. Autoinducer 2-dependent Escherichia coli biofilm formation is enhanced in a dual-species coculture. *Appl. Environ. Microbiol.* **84**, (2018).

21. Thompson, J. A., Oliveira, R. A., Ubeda, C., Xavier, K. B. & Djukovic, A. Manipulation

of the Quorum Sensing Signal AI-2 Affects the Antibiotic-Treated Gut Microbiota. *CellReports* **10**, 1861–1871 (2015).

22. Hsiao, A. *et al.* Members of the human gut microbiota involved in recovery from Vibrio cholerae infection. *Nature* **515**, 423–426 (2014).

23. Wotzka, S. Y. *et al.* Microbiota stability in healthy individuals after single-dose lactulose challenge—A randomized controlled study. *PLoS One* **13**, e0206214 (2018).

24. Jensen, K. F. The Escherichia coli K-12 'wild types' W3110 and MG1655 have an rph frameshift mutation that leads to pyrimidine starvation due to low pyrE expression levels. *J. Bacteriol.* **175**, 3401–3407 (1993).

25. Blattner, F. R. *et al.* The complete genome sequence of Escherichia coli K-12. *Science* vol. 277 1453–1462 (1997).

26. Soupene, E. *et al.* Physiological studies of Escherichia coli strain MG1655: Growth defects and apparent cross-regulation of gene expression. *J. Bacteriol.* **185**, 5611–5626 (2003).

27. Hobman, J. L., Penn, C. W. & Pallen, M. J. Laboratory strains of Escherichia coli: model citizens or deceitful delinquents growing old disgracefully? *Mol. Microbiol.* **64**, 881–885 (2007).

28. Leatham, M. P. *et al.* Precolonized human commensal Escherichia coli strains serve as a barrier to E. coli O157:H7 growth in the streptomycin-treated mouse intestine. *Infect. Immun.* **77**, 2876–2886 (2009).

29. Stecher, B. *et al.* Flagella and chemotaxis are required for efficient induction of Salmonella enterica serovar typhimurium colitis in streptomycin-pretreated mice. *Infect. Immun.* **72**, 4138–4150 (2004).

30. Stecher, B. *et al.* Motility allows S. Typhimurium to benefit from the mucosal defence. *Cellular Microbiology* vol. 10 1166–1180 (2008).

31. Thompson, J. A., Oliveira, R. A. & Xavier, K. B. Chemical conversations in the gut microbiota. *Gut Microbes* **7**, 163–170 (2016).

32. González Barrios, A. F. *et al.* Autoinducer 2 controls biofilm formation in Escherichia coli through a novel motility quorum-sensing regulator (MqsR, B3022). *J. Bacteriol.* **188**, 305–16 (2006).

33. Bansal, T., Jesudhasan, P., Pillai, S., Wood, T. K. & Jayaraman, A. Temporal regulation of enterohemorrhagic Escherichia coli virulence mediated by autoinducer-2.

Appl. Microbiol. Biotechnol. **78**, 811–819 (2008).

34. Xavier, K. B. & Bassler, B. L. Regulation of uptake and processing of the quorum-sensing autoinducer AI-2 in Escherichia coli. *J. Bacteriol.* **187**, 238–48 (2005).

35. Xavier, K. B. *et al.* Phosphorylation and Processing of the Quorum-Sensing Molecule Autoinducer-2 in Enteric Bacteria. *ACS Chem. Biol.* **2**, 128–136 (2007).

36. Hegde, M. *et al.* Chemotaxis to the quorum-sensing signal AI-2 requires the Tsr chemoreceptor and the periplasmic LsrB AI-2-binding protein. *J. Bacteriol.* **193**, 768–773 (2011).

37. Neumann, S., Hansen, C. H., Wingreen, N. S. & Sourjik, V. Differences in signalling by directly and indirectly binding ligands in bacterial chemotaxis. *EMBO J.* **29**, 3484–3495 (2010).

38. Oliveira, R. A. *et al.* Klebsiella michiganensis transmission enhances resistance to Enterobacteriaceae gut invasion by nutrition competition. *Nat. Microbiol. 2020 54* **5**, 630–641 (2020).

39. Luo, C. *et al.* ConStrains identifies microbial strains in metagenomic datasets. *Nat. Biotechnol. 2015 3310* **33**, 1045–1052 (2015).

40. Tyakht, A. V. *et al.* Genetic diversity of Escherichia coli in gut microbiota of patients with Crohn's disease discovered using metagenomic and genomic analyses. *BMC Genomics* **19**, 1–14 (2018).

41. Pereira, F. C. & Berry, D. Microbial nutrient niches in the gut. *Environ. Microbiol.* **19**, 1366–1378 (2017).

42. Conway, T. & Cohen, P. S. Commensal and Pathogenic Escherichia coli Metabolism in the Gut . *Microbiol. Spectr.* **3**, (2015).

43. Meador, J. P., Caldwell, M. E., Cohen, P. S. & Conway, T. Escherichia coli pathotypes occupy distinct niches in the mouse intestine. *Infect. Immun.* **82**, 1931–1938 (2014).

44. Brito, P. H., Rocha, E. P. C., Xavier, K. B. & Gordo, I. Natural Genome Diversity of AI-2 Quorum Sensing in Escherichia coli: Conserved Signal Production but Labile Signal Reception. *Genome Biol. Evol.* **5**, 16–30 (2013).

45. Stecher, B. *et al.* Gut inflammation can boost horizontal gene transfer between pathogenic and commensal Enterobacteriaceae. *Proc. Natl. Acad. Sci. U. S. A.* **109**, 1269–1274 (2012).

46. Riley, M. A. & Gordon, D. M. The ecological role of bacteriocins in bacterial

competition. *Trends Microbiol.* **7**, 129–133 (1999).

47. Marques, J. C. *et al.* LsrF, a coenzyme A-dependent thiolase, catalyzes the terminal step in processing the quorum sensing signal autoinducer-2. *Proc. Natl. Acad. Sci.* **111**, 14235–14240 (2014).

48. Laganenka, L. *et al.* Quorum Sensing and Metabolic State of the Host Control Lysogeny-Lysis Switch of Bacteriophage T1. *MBio* **10**, (2019).

49. Schembri, M. A., Hjerrild, L., Gjermansen, M. & Klemm, P. Differential Expression of the Escherichia coli Autoaggregation Factor Antigen 43. *J. Bacteriol.* **185**, 2236–2242 (2003).

50. Horesh, G. *et al.* A comprehensive and high-quality collection of escherichia coli genomes and their genes. *Microb. Genomics* **7**, 1–15 (2021).

51. Wiame, E., Delpierre, G., Collard, F. & Van Schaftingen, E. Identification of a Pathway for the Utilization of the Amadori Product Fructoselysine in Escherichia coli. *J. Biol. Chem.* **277**, 42523–42529 (2002).

52. Erbersdobler, H. F. & Faist, V. Metabolic transit of Amadori products. doi:10.1002/1521-3803.

53. Wolf, A. R. *et al.* Bioremediation of a Common Product of Food Processing by a Human Gut Bacterium. *Cell Host Microbe* **26**, 463-477.e8 (2019).

54. Barroso-Batista, J. *et al.* Specific Eco-evolutionary Contexts in the Mouse Gut Reveal Escherichia coli Metabolic Versatility. *Curr. Biol.* **30**, 1049-1062.e7 (2020).

55. Frazão, N., Sousa, A., Lässig, M. & Gordo, I. Horizontal gene transfer overrides mutation in Escherichia coli colonizing the mammalian gut. *Proc. Natl. Acad. Sci. U. S. A.* **116**, 17906–17915 (2019).

56. Sourjik, V. & Berg, H. C. Functional interactions between receptors in bacterial chemotaxis. **428**, 1–4 (2004).

57. Sourjik, V. & Berg, H. C. Receptor sensitivity in bacterial chemotaxis. *Proc. Natl. Acad. Sci. U. S. A.* **99**, 123–127 (2002).

58. Sourjik, V., Vaknin, A., Shimizu, T. S. & Berg, H. C. In vivo measurement by FRET of pathway activity in bacterial chemotaxis. *Methods Enzymol.* **423**, 365 (2007).

59. Laganenka, L., López, M. E., Colin, R. & Sourjik, V. Flagellum-Mediated Mechanosensing and RflP Control Motility State of Pathogenic Escherichia coli. *MBio* **11**, (2020).

60. Somavanshi, R., Ghosh, B. & Sourjik, V. Sugar Influx Sensing by the Phosphotransferase System of Escherichia coli. *PLOS Biol.* **14**, e2000074 (2016).

61. Ortega, Á., Zhulin, I. B. & Krell, T. Sensory Repertoire of Bacterial Chemoreceptors. *Microbiol. Mol. Biol. Rev.* **81**, (2017).

62. Wang, L., Hashimoto, D., Tsao, C. Y., Valdes, J. J. & Bentley, W. E. Cyclic AMP (cAMP) and cAMP receptor protein influence both synthesis and uptake of extracellular autoinducer 2 in Escherichia coli. *J. Bacteriol.* **187**, 2066–2076 (2005).

63. Ha, J.-H. *et al.* Evidence of link between quorum sensing and sugar metabolism in Escherichia coli revealed via cocrystal structures of LsrK and HPr. *Sci. Adv.* **4**, eaar7063 (2018).

64. Graf von Armansperg, B. *et al.* Transcriptional regulation of the Nε-fructoselysine metabolism in Escherichia coli by global and substrate-specific cues. *Mol. Microbiol.* **115**, 175–190 (2021).

65. Pereira, C. S. *et al.* Phosphoenolpyruvate phosphotransferase system regulates detection and processing of the quorum sensing signal autoinducer-2. *Mol. Microbiol.* **84**, 93–104 (2012).

66. Adler, J. Chemotaxis in bacteria. *Science* **153**, 708–716 (1966).

67. Koster, D. A., Mayo, A., Bren, A. & Alon, U. Surface growth of a motile bacterial population resembles growth in a chemostat. *J. Mol. Biol.* **424**, 180–191 (2012).

68. Laganenka, L. & Sourjik, V. Autoinducer 2-dependent Escherichia coli biofilm formation is enhanced in a dual-species co-culture. *Appl. Environ. Microbiol.* AEM.02638-17 (2017) doi:10.1128/AEM.02638-17.

69. Gauger, E. J. *et al.* Role of motility and the flhDC Operon in Escherichia coli MG1655 colonization of the mouse intestine. *Infect. Immun.* **75**, 3315–3324 (2007).

70. de Paepe, M. *et al.* Trade-off between bile resistance and nutritional competence drives Escherichia coli diversification in the mouse gut. *PLoS Genet.* **7**, (2011).

71. Monday, S. R., Minnich, S. A. & Feng, P. C. H. A 12-Base-Pair Deletion in the Flagellar Master Control Gene flhC Causes Nonmotility of the Pathogenic German Sorbitol-Fermenting Escherichia coli O157:H- Strains. *J. Bacteriol.* **186**, 2319–2327 (2004).

72. Rossmann, F. S. *et al.* Phage-mediated dispersal of biofilm and distribution of bacterial virulence genes is induced by quorum sensing. *PLoS Pathog.* **11**, e1004653 (2015).

73. Anderson, J. K. *et al.* Chemorepulsion from the Quorum Signal Autoinducer-2 Promotes Helicobacter pylori Biofilm Dispersal. *MBio* **6**, e00379 (2015).

74. Rader, B. A. *et al.* Helicobacter pylori perceives the quorum-sensing molecule AI-2 as a chemorepellent via the chemoreceptor TlpB. *Microbiology* **157**, 2445–55 (2011).

75. Conway, T. & Cohen, P. S. Applying the restaurant hypothesis to intestinal microbiota: Anaerobes in mixed biofilms degrade polysaccharides, sharing locally prepared sugars with facultative anaerobes that also colonize the intestine. *Microbe* **10**, 324–328 (2015).

76. Long, Z., Quaife, B., Salman, H. & Oltvai, Z. N. Cell-cell communication enhances bacterial chemotaxis toward external attractants. *Sci. Reports 2017 71* **7**, 1–12 (2017).

77. Molloy, M. J. *et al.* Intraluminal containment of commensal outgrowth in the gut during infection-induced dysbiosis. *Cell Host Microbe* **14**, 318–328 (2013).

78. Haag, L. M. *et al.* Intestinal microbiota shifts towards elevated commensal Escherichia coli loads abrogate colonization resistance against Campylobacter jejuni in mice. *PLoS One* **7**, (2012).

79. Spees, A. M. *et al.* Streptomycin-induced inflammation enhances Escherichia coli gut colonization through nitrate respiration. *MBio* **4**, (2013).

80. Carvalho, F. A. *et al.* Transient inability to manage proteobacteria promotes chronic gut inflammation in TLR5-deficient mice. *Cell Host Microbe* **12**, 139–152 (2012).

81. Datsenko, K. A. & Wanner, B. L. One-step inactivation of chromosomal genes in Escherichia coli K-12 using PCR products. *Proc. Natl. Acad. Sci. U. S. A.* **97**, 6640–6645 (2000).

82. Cherepanov, P. P. & Wackernagel, W. Gene disruption in Escherichia coli: TcR and KmR cassettes with the option of Flp-catalyzed excision of the antibiotic-resistance determinant. *Gene* **158**, 9–14 (1995).

83. Furter, M., Sellin, M. E., Hansson, G. C. & Hardt, W. D. Mucus Architecture and Near-Surface Swimming Affect Distinct Salmonella Typhimurium Infection Patterns along the Murine Intestinal Tract. *Cell Rep.* **27**, 2665-2678.e3 (2019).

84. Valdivia, R. H. & Falkow, S. Bacterial genetics by flow cytometry: rapid isolation of Salmonella typhimurium acid-inducible promoters by differential fluorescence induction. *Mol. Microbiol.* **22**, 367–378 (1996).

85. Barthel, M. *et al.* Pretreatment of mice with streptomycin provides a Salmonella

enterica serovar Typhimurium colitis model that allows analysis of both pathogen and host. *Infect. Immun.* **71**, 2839–2858 (2003).

86. Miller, K. A., Phillips, R. S., Kilgore, P. B., Smith, G. L. & Hoover, T. R. A Mannose Family Phosphotransferase System Permease and Associated Enzymes Are Required for Utilization of Fructoselysine and Glucoselysine in Salmonella enterica Serovar Typhimurium. *J. Bacteriol.* **197**, 2831–2839 (2015).

87. Hyatt, D. *et al.* Prodigal: prokaryotic gene recognition and translation initiation site identification. (2010).

88. Seemann, T. Prokka: rapid prokaryotic genome annotation. *Bioinformatics* **30**, 2068–2069 (2014).

89. Lees, J. A. *et al.* Fast and flexible bacterial genomic epidemiology with PopPUNK. *Genome Res.* **29**, 304–316 (2019).

90. Johnson, M. *et al.* NCBI BLAST: a better web interface. *Nucleic Acids Res.* **36**, (2008).

91. Mckinney, W. pandas: a Foundational Python Library for Data Analysis and Statistics.

92. Szklarczyk, D. *et al.* The STRING database in 2021: customizable protein-protein networks, and functional characterization of user-uploaded gene/measurement sets. *Nucleic Acids Res.* **49**, D605–D612 (2021).

93. Huerta-Cepas, J., Serra, F. & Bork, P. ETE 3: Reconstruction, Analysis, and Visualization of Phylogenomic Data. *Mol. Biol. Evol.* **33**, 1635–1638 (2016).

94. Menardo, F. *et al.* Treemmer: A tool to reduce large phylogenetic datasets with minimal loss of diversity. *BMC Bioinformatics* **19**, 1–8 (2018).

95. Harris, C. R. *et al.* Array programming with NumPy. *Nat. 2020 5857825* **585**, 357–362 (2020).

Acknowledgements

We are grateful to Karina Xavier (Instituto Gulbenkian de Ciência, Oeiras, Portugal) for generously providing *E. coli* ARO071 strain and for helpful discussions. We further thank the RCHCI staff for support of the animal work. L.L. is supported by LA 4572/1-1 grant from the Deutsche Forschungsgemeinschaft. This work has been further funded by grants from the Swiss National Science Foundation (310030B_173338, 310030_192567, NCCR Microbiomes) to W.-D.H. V.S. acknowledges support by the Hessian Ministry of Higher Education, Research, and the Arts (HMWK)–LOEWE research cluster “Diffusible Signals” subproject A1. J.W.L. was supported by the grant NRF-2019R1A6A3A03031885 from National Research Foundation,

Republic of Korea. C.v.M. is supported by the Swiss National Science Foundation (310030_192569). C.L.D. and J.P. are supported by SNF 205321L_10724 grant from the Swiss National Science Foundation .

Author information

Affiliations

Institute of Microbiology, D-BIOL, ETH Zurich, Zurich, Switzerland

Leanid Laganenka, Cora Dieterich, Lea Fuchs, Jörn Piel, Wolf-Dietrich Hardt

Max Planck Institute for Terrestrial Microbiology and LOEWE Center for Synthetic Microbiology (SYNMIKRO), Marburg, Germany

Jae-Woo Lee, Victor Sourjik

Department of Molecular Life Sciences and SIB Swiss Institute of Bioinformatics, University of Zurich, Zurich, Switzerland

Lukas Malfertheiner, Christian von Mering

Contributions

L.L., W.-D.H. and V.S. conceived and designed the experiments, L.L. and J.-W.L. performed the experiments, L.M. and C. v. M. performed bioinformatic analysis, C.L.D., L.F. and J.P. synthesized fructoselysine. All authors contributed to data analysis and writing of the manuscript.

Corresponding author

Correspondence to Wolf-Dietrich Hardt, wolf-dietrich.hardt@micro.biol.ethz.ch

Ethics declarations

Competing interests

The authors declare no competing interests

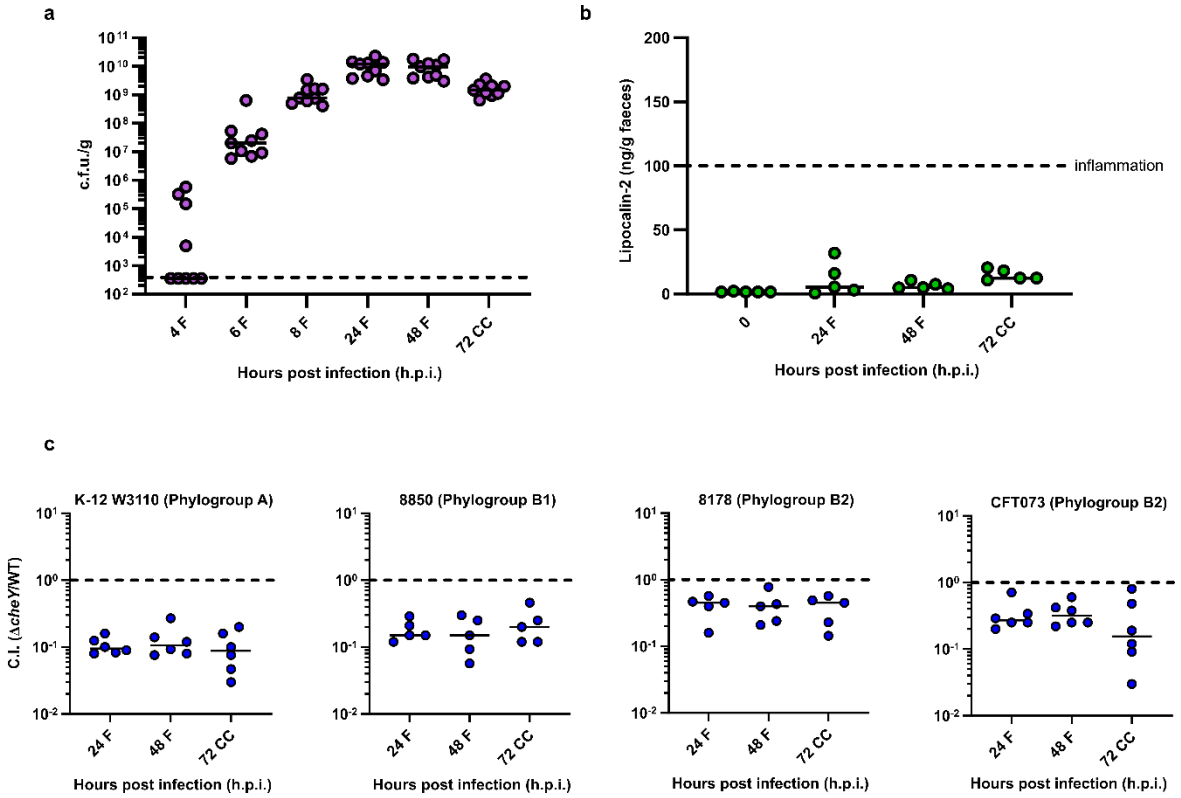

Extended Data Figure 1. *E. coli* Z1331 colonizes ampicillin-pretreated SPF mice without causing inflammation. a, c.f.u. of *E. coli* Z1331 WT (*yidX-bla*, amp^r) detected in faeces (F) and caecal content (CC) of ampicillin-pretreated SPF mice at different time points of a 72 h infection. Lines indicate median values (n=9, from ≥2 independent animal experiments). The slight drop of fecal *E. coli* densities between 48 h and 72 h.p.i. is likely due to the regrowth of microbiota. The dashed line indicates the detection limit. **b**, Lipocalin-2 levels in faeces (F) and caecal content (CC) of *E. coli*-infected mice as measured by ELISA. Lines represent median values (n=5, from ≥2 independent animal experiments). Dashed line indicates approximate threshold of lipocalin-2 concentration marking a shift from non-inflamed to the inflamed gut, as observed in the streptomycin mouse model for *Salmonella* diarrhea[1,2]. Note that gut colonization by wild type *S*. Typhimurium yields lipocalin-2 levels of 10^4 ng/g faeces during full-blown gut inflammation[1]. **c**, Competitive indices (C.I.) for chemotaxis-deficient Δ*cheY* strains from different phylogroups in competition against the respective WT strains in SPF ampicillin-pretreated mice. F, faeces. CC, caecal content. Lines indicate median values (min n=5, at least two independent replicates).

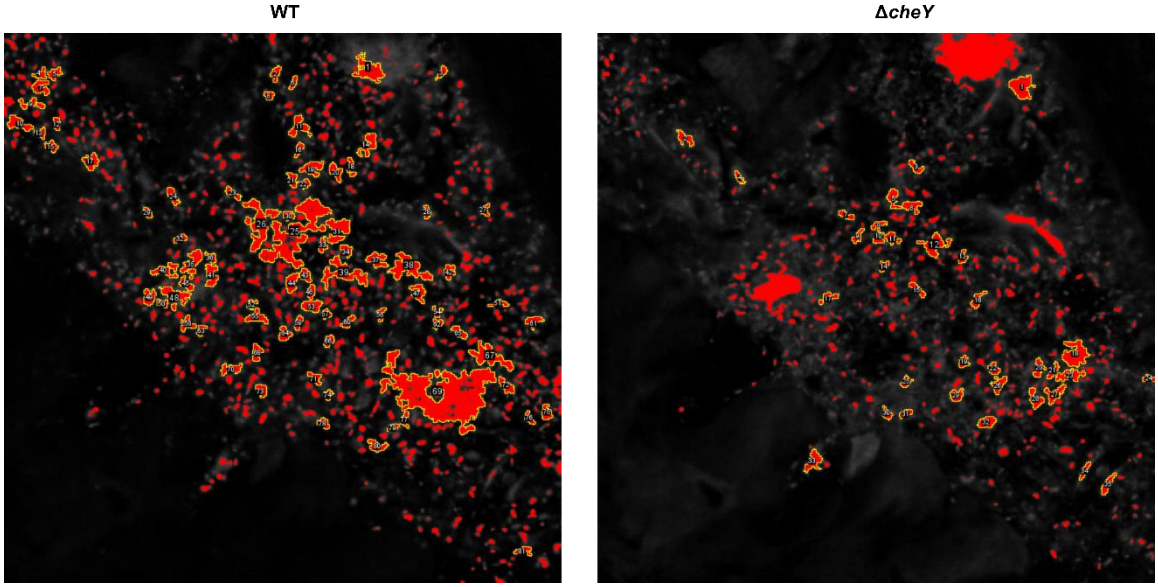

Extended Data Figure 2. An example of image segmentation and analysis of bacterial aggregates (as seen in Fig. 1d) using ImageJ. Detected particles are indicated in red, with aggregates (at least 50 px^2 in size) outlined in yellow. Particles of non-bacterial origin (food fibers etc, as seen in Δ*cheY* panel) were manually excluded from analysis.

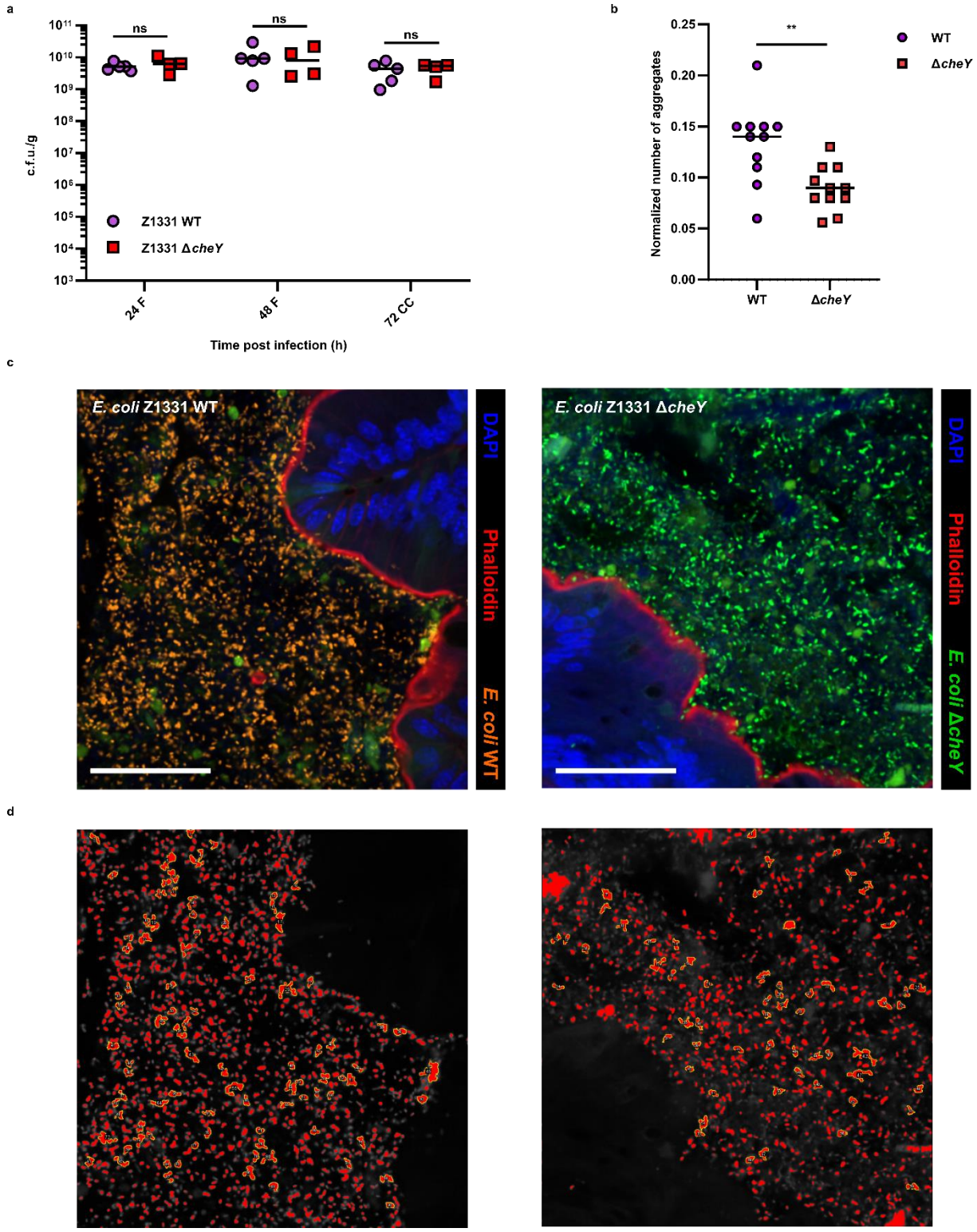

Extended Data Figure 3. *E. coli* Z1331 Δ*cheY* has no colonization defect in single-strain infection. a, , c.f.u. of *E. coli* Z1331 WT and Δ*cheY* detected in faeces (F) and caecal content (CC) of ampicillin-pretreated SPF mice at different time points of a 72 h infection. Lines indicate median values (n=4, 2 independent replicates). **b**, Number of aggregates formed by WT and Δ*cheY* cells in a single-strain infection normalized to the number of detected cells in a tissue section as seen below (Mann-Whitney test, ***P*<0.005). Lines

indicate median values (n=11, tissues sections from two independent experiments were analyzed). **c**, Caecal tissue sections of mice infected either with *E. coli* WT (mCherry-positive, shown in orange) or Δ*cheY* (GFP-positive, shown in green) at 72 h.p.i. Actin filaments (red) and DNA (blue) were stained with phalloidin and DAPI, respectively. Scale bars, 50 µm. **d**, An example of image segmentation and analysis of bacterial aggregates (as seen above) using ImageJ. Detected particles are indicated in red, with aggregates (at least 50 px^2 in size) outlined in yellow. Particles of non-bacterial origin (food fibers etc, as seen in Δ*cheY* panel) were manually excluded from analysis.

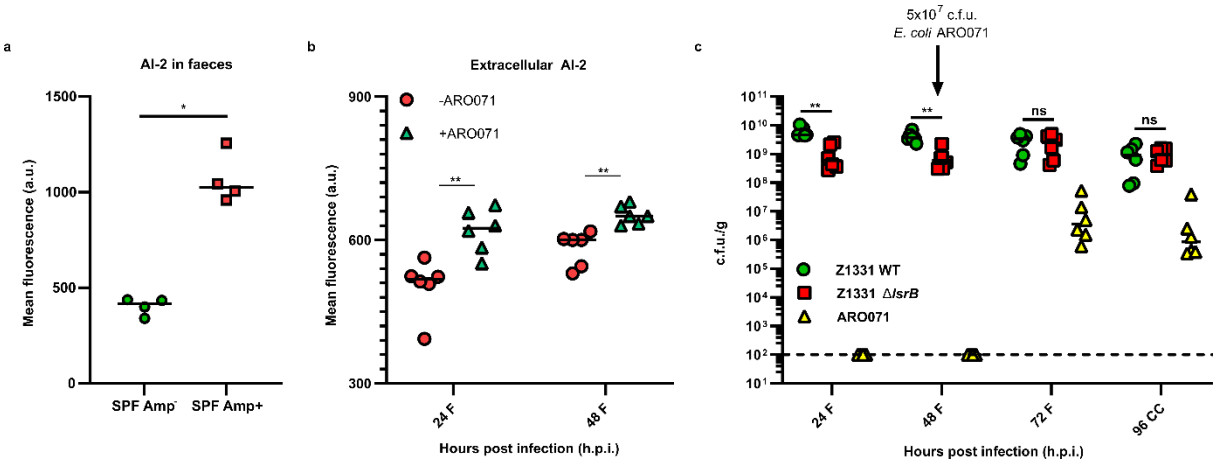

Extended Data Figure 4. Increased luminal AI-2 levels abolish fitness advantage of wild-type *E. coli* in Δ*lsrB*/WT competitive infection. a, AI-2 levels of AI-2 in faeces of SPF mice before (SPF Amp$^-$) and 24 h after (SPF Amp$^+$) treatment with 20 mg ampicillin. Mean fluorescence of a plasmid-based AI-2 reporter strain was measured by flow cytometry and plotted in arbitrary units (a.u.). Lines indicate median values (n=4, at least two independent replicates). *P* values were calculated using the Mann-Whitney test (**P*<0.05). **b**, AI-2 levels of AI-2 in faeces (F) of SPF ampicillin-pretreated mice infected with *E. coli* Z1331 WT (-ARO071) or with 1:1 mix of *E. coli* Z1331 WT and *E. coli* ARO071. Mean fluorescence of a plasmid-based AI-2 reporter strain was measured by flow cytometry and plotted in arbitrary units (a.u.). Lines indicate median values (n=6, at least two independent replicates). *P* values were calculated using the Mann-Whitney test (***P*<0.005). **c**, c.f.u. data for the experiment shown in Fig. 2d. F, faeces, CC, caecal content. Lines indicate median values (n=6, at least two independent replicates). *P* values were calculated using Mann-Whitney test (***P*<0.005; ns, not significant). The dashed line indicates the detection limit. Note that the total c.f.u. loads can differ between caecum and faeces due to yet unidentified reasons.

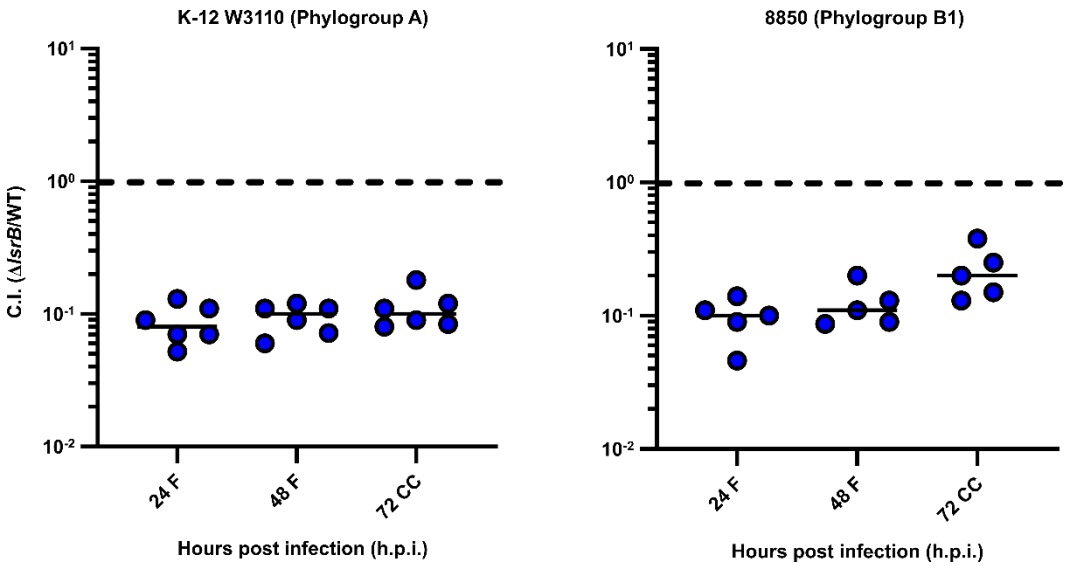

Extended Data Figure 5. Competitive indices (C.I.) for Δ*lsrB* strains of *lsr*-positive *E. coli* W3110 and 8550 in competition against the respective WT strains in SPF ampicillin-pretreated mice. F, faeces. CC, caecal content. Lines indicate median values (min n=5, at least two independent replicates).

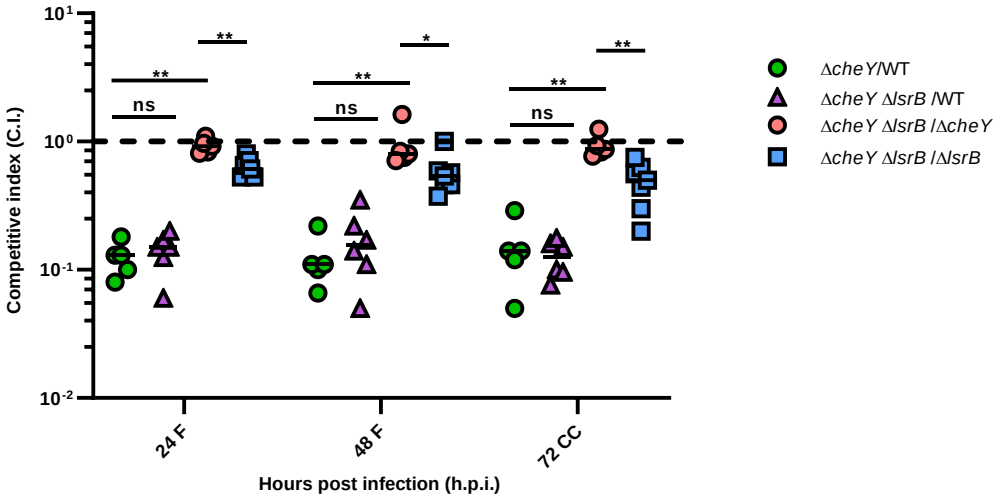

Extended Data Figure 6. CheY and LsrB belong to the same regulatory pathway. *E. coli* Z1331 Δ*cheY* and Δ*cheY* Δ*lsrB* knockout strains were competed against the wild-type strain. Additionally competitive indices (C.I.) of Δ*lsrB* and Δ*cheY* mutants were analyzed in Δ*cheY* and Δ*lsrB* backgrounds, respectively. F, faeces, CC, caecal content. Lines indicate median values (min n=5, from at least two independent infection experiments). *P* values were analyzed using the Mann-Whitney test (***P*<0.005; **P*<0.05; ns, not significant)

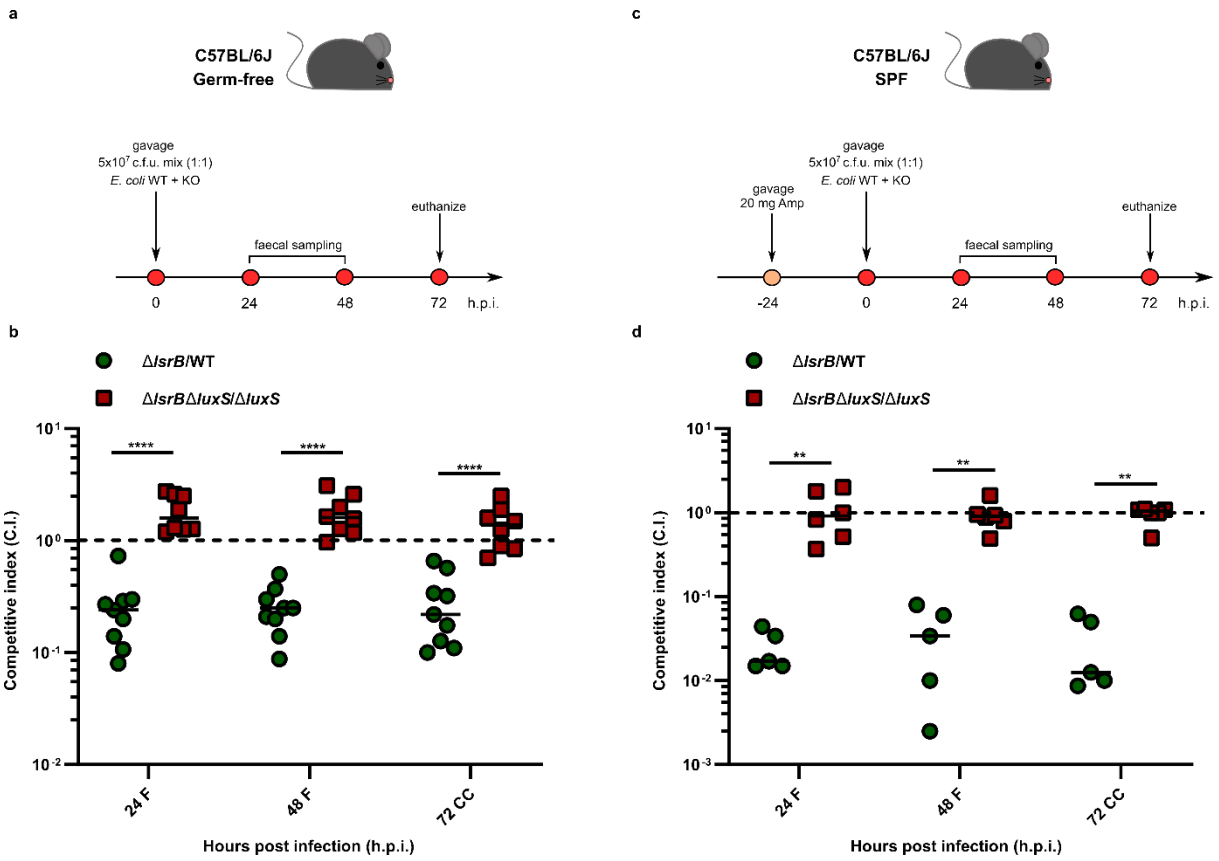

Extended Data Figure 7. Self-produced AI-2 enhances gut colonization by *E. coli*. a, Experimental scheme of competitive infection in germ-free (GF) mice. C57BL/6J GF mice were orally infected with $5x10^7$ c.f.u. *E. coli* W3110 WT and Δ*lsrB* or Δ*lsrB* Δ*luxS* and Δ*luxS* at a 1:1 ratio. Faeces were collected 24, 48 h.p.i. and mice were euthanized at 72 h.p.i. **b**, C.I. of non-AI-2 chemotactic Δ*lsrB* mutant in WT and Δ*luxS* background strains in the GF mouse infection model. F, faeces, CC, caecal content. Lines indicate median values (n=9, from least two independent experiments). *P* values were calculated using the Mann-Whitney test (****$P<0.0001$). **c**, Experimental scheme of competitive infection in SPF mice. C57BL/6J SPF mice were pretreated with 20 mg ampicillin by oral gavage 24 h prior to infection with *E. coli* W3110 WT and Δ*lsrB* or Δ*lsrB* Δ*luxS* and Δ*luxS* at 1:1 ratio. Faeces were collected at 24, 48 h.p.i and mice were euthanized at 72 h.p.i. **d,** C.I. of non-AI-2 chemotactic Δ*lsrB* mutant in WT and Δ*luxS* background strains in SPF ampicillin-pretreated mouse infection model. F, faeces, CC, caecal content. Lines indicate median values (min n=5, from at least two independent experiments). *P* values were calculated using the Mann-Whitney test (**$P<0.005$).

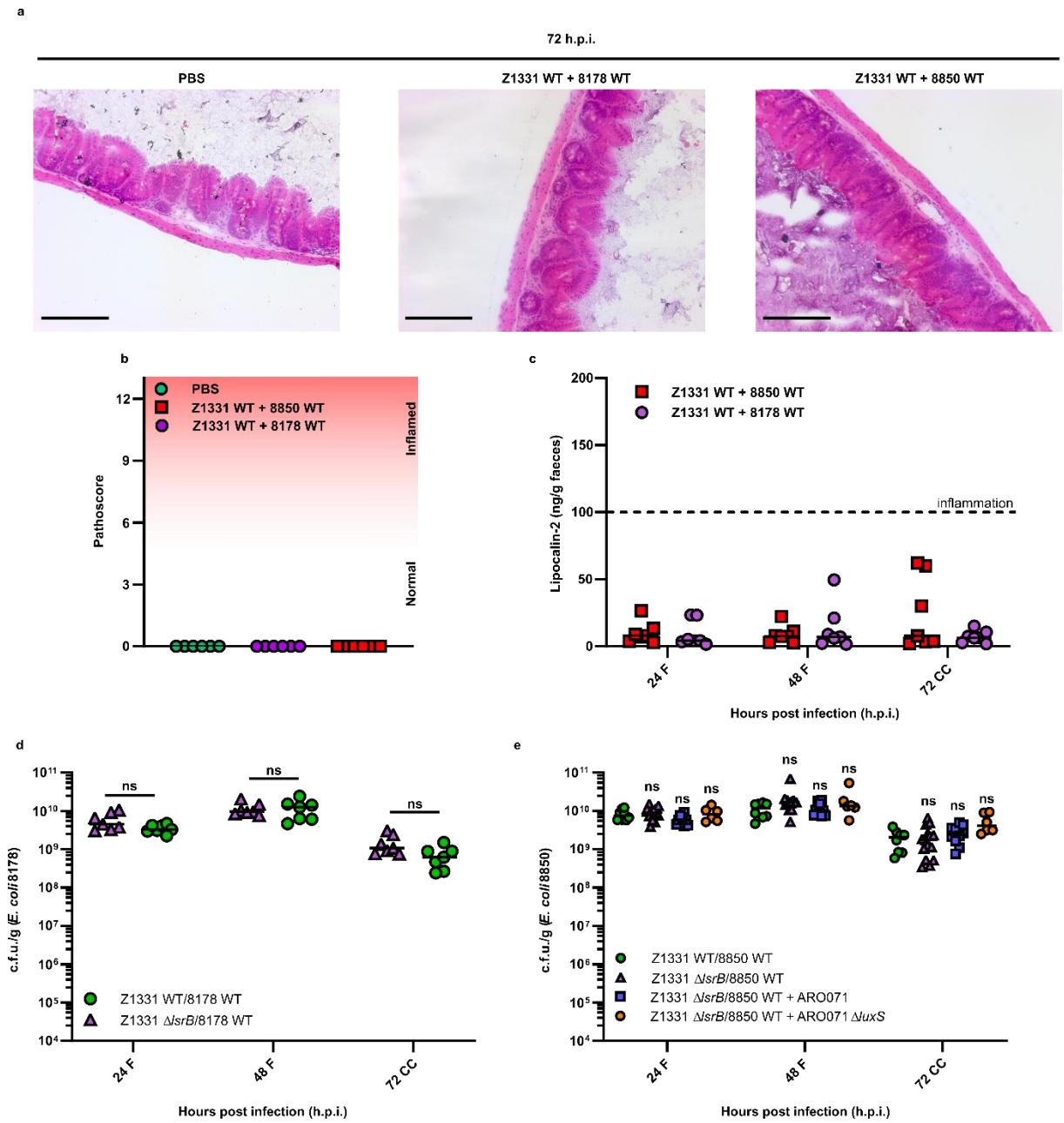

Extended Data Figure 8. Infection of SPF ampicillin-pretreated mice with *E. coli* 8178 and 8850 does not cause inflammation. a, H&E staining of caecal tissue of uninfected mice (PBS) and mice infected with $5x10^7$ c.f.u. of *E. coli* Z1331 WT + 8178 WT and *E. coli* Z1331 WT + 8850 WT (1:1000 ratio) at 72 h.p.i (as seen in Fig. 4). Scale bar, 50 µm. **b**, Histopathology analysis of the caecal tissue section as seen above. 3 sections from 2 mice per group were analyzed. **c**, Lipocalin-2 levels in faeces (F) and caecal content (CC) of *E. coli*-infected mice as measured by ELISA. Lines represent median values (n=7, at least two independent animal experiments). Dashed line indicates approximate threshold of lipocalin-2 concentration marking a shift from non-inflamed to the inflamed gut. **d**, Colonization levels of *E. coli* 8178 in competition experiments with *E. coli* Z1331 as seen in Fig. 2. Lines indicate median values (n=7, at least two independent replicates). *P* values were calculated using the Mann-Whitney test (ns, not significant). **e**, Colonization levels of *E. coli* 8850 in competition experiments with *E. coli* Z1331 as seen in Fig. 2. Lines indicate median values (min n=6, at least two independent replicates). *P* values were calculated using the Mann-Whitney test (ns, not significant).

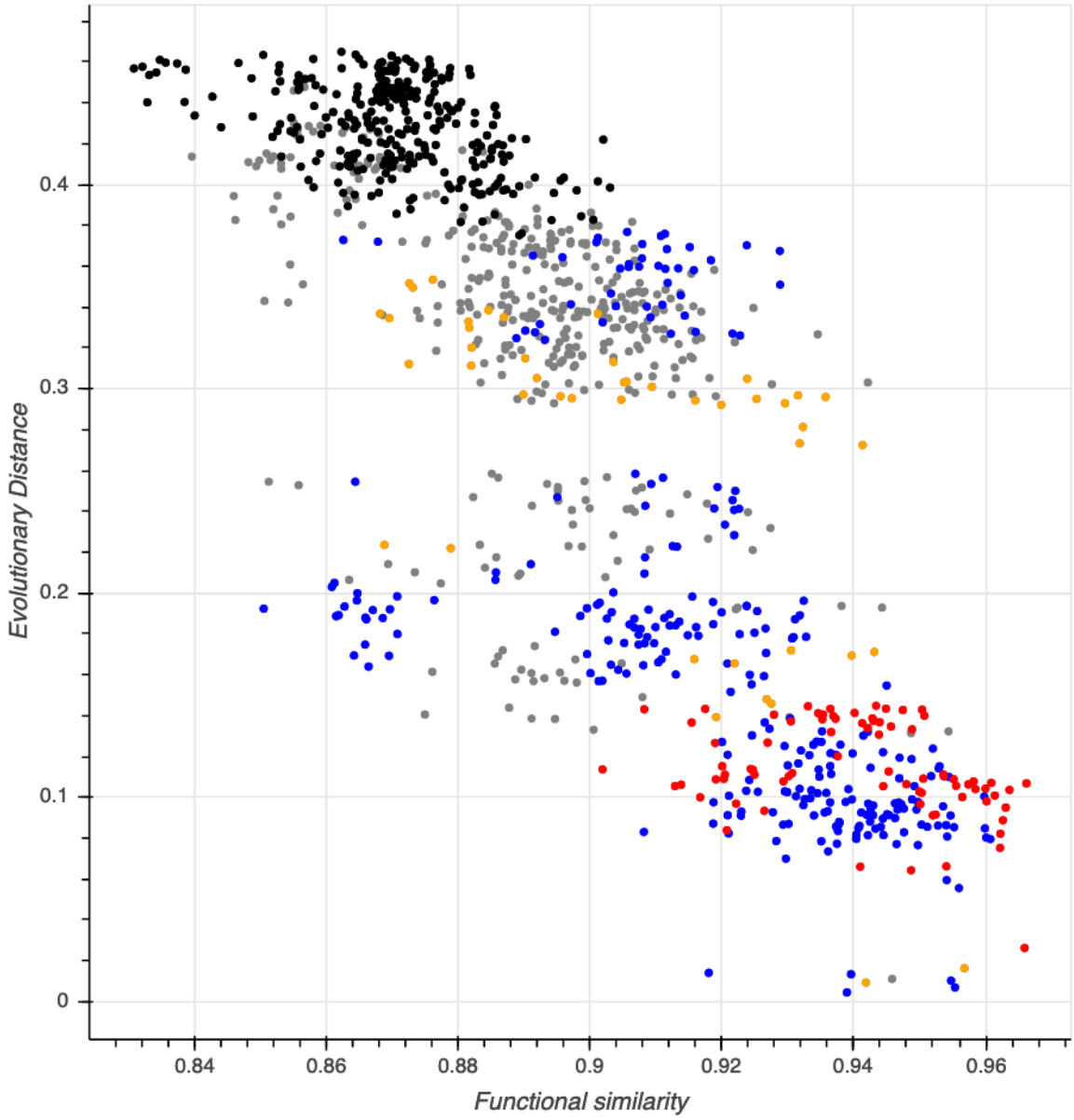

Extended Data Figure 9. *E. coli* genomes containing both *lsrB* and *frlA* are more closely related to each other than the average *E. coli* genomes. *E. coli* lineages were split up into three groups. Group 1 contains both *frlA* and *lsrB*, group 2 contains neither *frlA* nor *lsrB* and group 3 contains either *frlA* or *lsrB*. Phylogenetic distance (based on tree branch lengths, Y-axis) was plotted against the fraction of shared annotated genes (x-axis) of the lineages in an all-against all manner and colored according to their groups. Blue dots indicate group 1 compared with group 1, red dots indicate group 2 compared with group 2, orange dots indicate group 3 compared against group 3, black dots indicate group 1 compared with group 2, and grey dots indicate group 3 against group 1 and group 2, respectively.

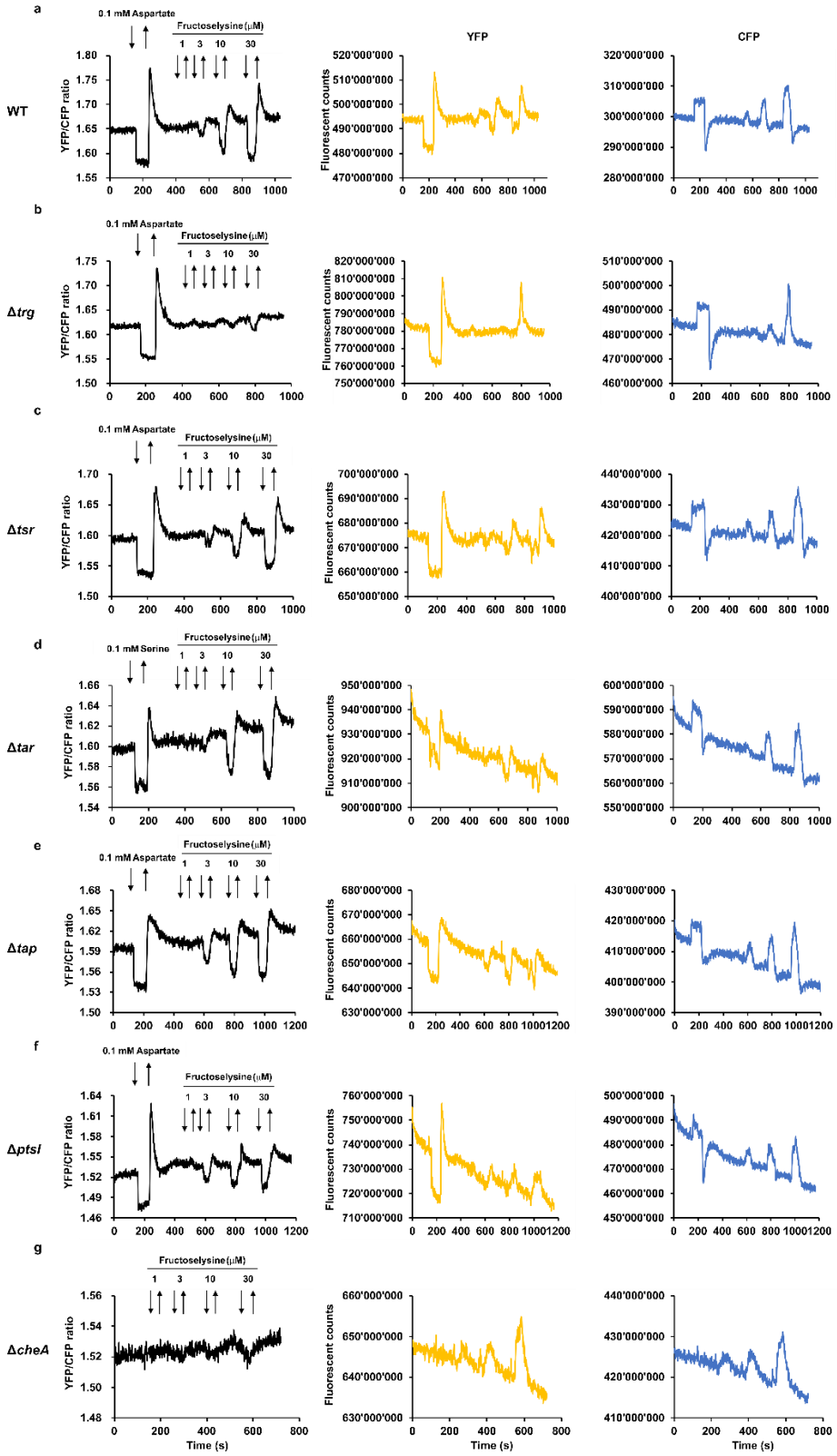

Extended Data Figure 10. Fructoselysine is an attractant sensed by the Trg chemoreceptor. Examples of FRET measurements of the response to fructoselysine by *E. coli* W3110 **a**, wild-type, **b**, Δ*trg*, **c**, Δ*tsr*, **d**, Δ*tar*, **e**, Δ*tap*, **f**, Δ*ptsI* and **g**, Δ*cheA* (negative control) knockout strains. Buffer-adapted cells were stimulated with step-like addition and removal of compounds (indicated by downward and upward arrows, respectively). Stimulation with saturating concentration of aspartate or serine, two strong attractants, was used as a positive control. Time traces of fluorescence intensity in the YFP and CFP channels are shown in the right. Opposite changes in two channels indicate specific FRET response. Note that

higher concentrations of fructoselysine solution have unspecific effect on fluorescence in both YFP and CFP channels, particularly visible in Δ*cheA* negative control, but little effect on the YFP/CFP ratio. Residual effect on the YFP/CFP ratio in the negative control was subtracted from all dose-response curves in Figure 4b.

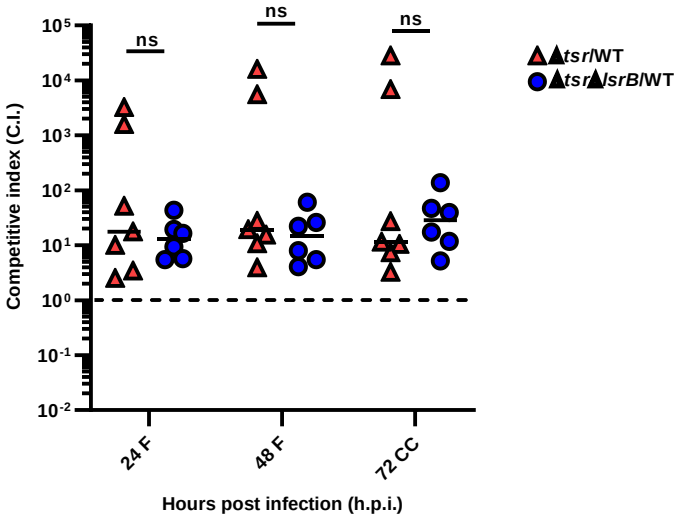

Extended Data Figure 11. LsrB and Tsr belong to the same regulatory pathway. Competitive indices (C.I.) of *E. coli* Δ*tsr* and Δ*tsr* Δ*lsrB* mutant strains vs the wild-type strain *E. coli* Z1331 in SPF ampicillin-pretreated mice. F, faeces, CC, caecal content. Lines indicate median values (min n=6, at least two independent replicates). *P* values were analyzed using the Mann-Whitney test (ns, not significant).

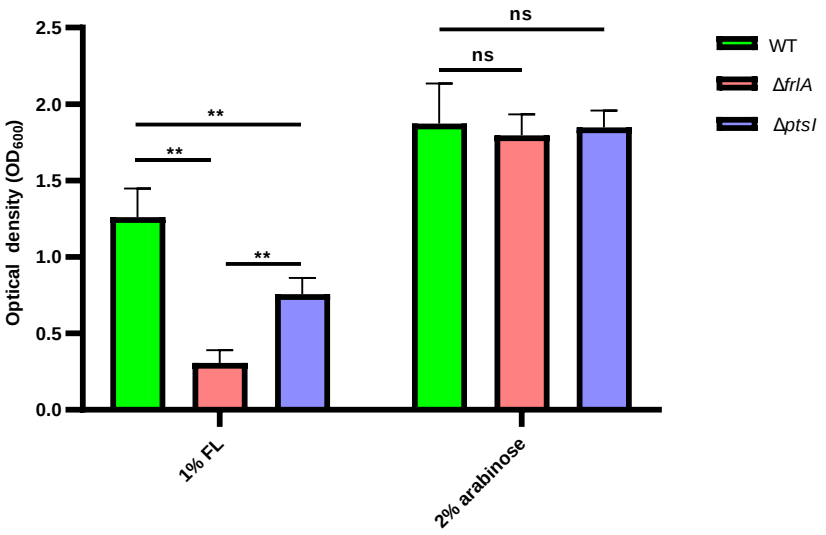

Extended Data Figure 12. *E. coli* Z1331 utilizes fructoselysine as a sole carbon source. *E. coli* Z1331 WT, Δ*frlA* and Δ*ptsI* strains were grown aerobically for 24 h in M9 minimal medium supplemented with either 1% fructoselysine (FL) or 2% arabinose (non-PTS sugar, used as a control for Δ*ptsI* growth) and NH_4Cl as a nitrogen source. Error bars indicate s.d. (n=6, from at least two independent experiments). *P* values were calculated using the Mann-Whitney test (**$P<0.005$; ns, not significant).

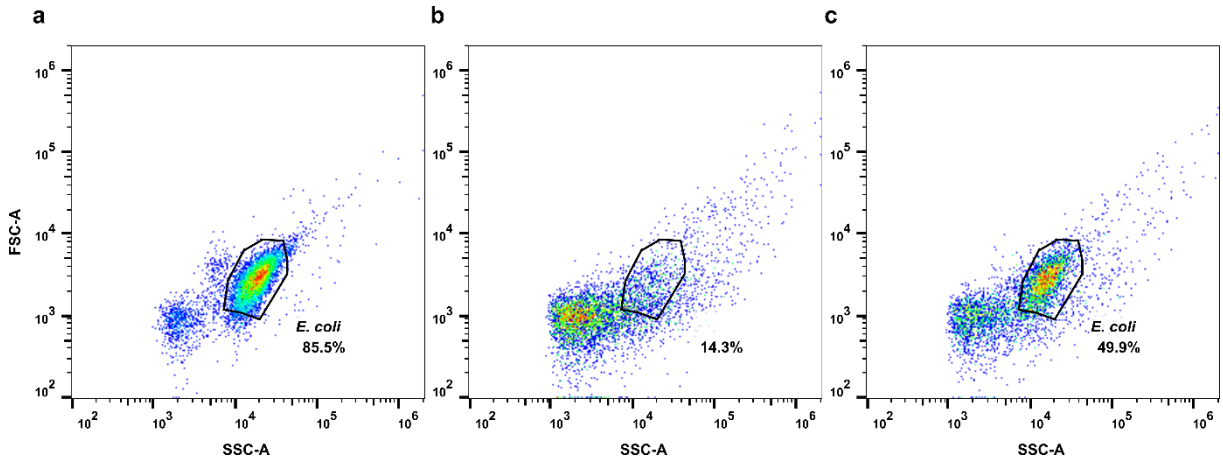

Extended Data Figure 13. Gating strategy for measuring E. coli gene expression in vitro and in vivo (as seen in Fig. 2a and Fig. 5a-c). Representative plots of forward versus side scatter gating of **a,** *in vitro E. coli* culture grown in TB, **b,** faeces sample of uninfected SPF mice 24 h after ampicillin treatment (negative control), **c,** *E. coli* in faeces of ampicillin-pretreated mice 24 h.p.i.

Supplementary References

1. Maier, L. *et al.* Microbiota-derived hydrogen fuels Salmonella typhimurium invasion of the gut ecosystem. *Cell Host Microbe* **14**, 641–651 (2013).

2. Nguyen, B. D. *et al.* Import of Aspartate and Malate by DcuABC Drives H2/Fumarate Respiration to Promote Initial Salmonella Gut-Lumen Colonization in Mice. *Cell Host Microbe* **27**, 922-936.e6 (2020).